UNIVERSITY OF OKLAHOMA

GRADUATE COLLEGE

HYDRAULIC FORCE MODELING FOR RADIAL JET DRILLING

A THESIS

SUBMITTED TO THE GRADUATE FACULTY

in partial fulfillment of the requirements for the

Degree of

MASTER OF SCIENCE

By

ANDREW WIECHMAN
Norman, Oklahoma
2018

HYDRAULIC FORCE MODELING FOR RADIAL JET DRILLING

A THESIS APPROVED FOR THE
MEWBOURNE SCHOOL OF PETROLEUM AND GEOLOGICAL ENGINEERING

BY

_____
Dr. Ramadan Ahmed, Chair

_____
Dr. Catalin Teodoriu

_____
Dr. Saeed Salehi

I dedicated to my friends and family that have provided tremendous support since showing up on campus at OU. Specifically, my mother Pam, my father Mike, and girlfriend Darri Beckwith, words cannot express how thankful I am to have their undying support. Others that supported me throughout this journey include my brother and sister, Doug and Kelly; Darrien's family with the father Darren, mother Lisa, sister Dani, sister Delaney, grandfather Keith, and grandmother Oleta; a few former classmates Thai Phi, James Moran and Sidarth Bagawandoss; friends John and Jake Moehlenbrock. I would like to also recognize the Louder with Crowder crew for helping me make light of many situations during some stressful times at school.

Acknowledgements

Words cannot express my gratitude to my advisor, Dr. Ramadan Ahmed for his guidance, patience, and support through the entirity of this research. I would like to thank Dr. Teodoriu and Dr. Salehi for their suggestions and considerations while working on this study. Also, I need to thank the folks at the WCTC who were always willing to help and offer any assistance when needed. I would like to thank Jeff McCaskill for his help and guidance, especially on the assembly of the testing set up. I need to thank Dr. Buckman from Buckman Jet Drilling for providing field and production data for this study.

Table of Contents

Table of Contents v
List of Tables vii
List of Figures viii
Abstract x
Chapter 1 – Introduction 1
1.1 Overview 1
1.2 Problem Statement 2
1.3 Objectives 3
1.4 Methodology 4
Chapter 2 – Literature Review 5
2.1 Application 5
2.2 Field Equipment and Procedure 7
2.3 Previous Studies 8
2.3.1 System Development 8
2.3.2 Field Studies 13
2.3.3 Theoretical Studies 19
Chapter 3 – Theoretical RJD 24
3.1 RJD Force Theory 24
3.2 Existing Models 25
3.2.1 Theoretical Model 1 26
3.2.2 Theoretical Model 2 33
Chapter 4 – Mathematical Modeling 39
4.1 Assumptions 39
4.2 Conservation of Mass 40
4.3 Conservation of Linear Momentum 41
4.4 Conservation of Angular Momentum 42
4.5 Energy Balance 43
4.6 Discharge Coefficient 45
Chapter 5 – Experimentation 48
5.1 Test Scope 48

5.2 Test Set-up 48
5.3 Test Procedure 50
5.4 Test Results 53
Chapter 6 – Parametric Study 57
Chapter 7 - Conclusions 64
Recommendations 66
References 69
Appendix 72

List of Tables

Table 2.1 – Oil and water production rate with and without RJD intervention 15
Table 2.2 – Production data before and after RJD (data from Cinelli and Kamel 2013) 17
Table 2.3 – Pre and Post RJD production data (courtesy of Dr. Buckman with BJD)....18
Table 3.1 – Numerical and calculated values of the self-propelled force (Li et al. 2015).....38
Table 5.1 – Nozzle Dimensions.....51
Table 5.2 – Nozzle Combinations 52

List of Figures

Fig. 2.1 - Schematic of the early RJD system (Dickinson et al. 1986) 11
Fig. 2.2 – RJD control while drilling setup (Dickinson et al. 1990) 11
Fig. 2.3 – BHA of the Buckman Jet Drilling system (Buckman et al. 2013).....12
Fig. 2.4 – Oil Production rate with and without RJD (data from Dickinson et al. 1993)14
Fig. 3.1 - Design of RJD bit (Bin et al. 2016) 24
Fig. 3.2 – Simple nozzle illustration of the forces in the system (Ruichang et al. 2009)27
Fig. 3.3 – Schematic of the experimental setup (Ruichang et al. 2009).....30
Fig. 3.4 –Pressure drop vs. flow rate (Ruichang et al. 2009) 31
Fig. 3.5 – The differential pressure coefficient vs. flow rate (Ruichang et al. 2009).....31
Fig. 3.6 - Pulling force vs flow rate for different hole sizes.....32
Fig. 3.7– Model predicted pulling force vs. flow rate for different hole sizes.....33
Fig. 3.8– Design of a multi-orifice nozzle (Li et al. 2015).....34
Fig. 3.9 – Schematic of test setup (Li et al. 2015).....37
Fig. 3.10 – Measured and calculated self-propelling force versus flow rates (Li et al. 2015).....38
Fig. 4.1 – Forces on the jet bit (adopted from Ruichang et al. 2009).....39
Fig. 4.2– Plot of aspect ratio vs discharge coefficient through orifices (data acquired from Lichtarowicz et al. (1965) and Ward-Smith (1971)) 46
Fig. 4.3 – Plotted data from Ward-Smith (1971) and Lichtarowicz (1965) with aspect ratios from 0-9.5 alongside Eq. 4.20-4.21. 47
Fig. 5.1 – Test loop schematic. 49
Fig. 5.2 – Microscopic photo of a brass nozzle with a reference stencil overlaid. 51
Fig. 5.3 – Chart of nozzle dimensions with 1-8 being front nozzles and 9-10 being back nozzles. 52
Fig. 5. 4 – Results for single orifice with a diameter of 1.585 mm and aspect ratio of 1.45: a) flow rate vs pressure; and b) backward force vs. pressure.....56
Fig. 5. 5 – Results for a single front orifice with a diameter of 1.433 mm and aspect ratio of 4.85: a) flow rate vs. pressure; and b) backward force vs. pressure 56
Fig. 5. 6 – Results for a nozzle with one front orifice with a diameter of 1.406 mm and aspect ratio of 1.64, and two back nozzles angled at 45-degree toward the back with diameters of 1.6 mm and aspect ratios of 3.75: a) flow rate vs. pressure; and b) propulsion force vs. pressure.....57
Fig. 6. 1 – Results using pressure data from Li et al. (2015) and a 6+3+1 nozzle configuration for various discharge coefficients; nozzle diameters set 1.2 mm diameter; front nozzles angle set to 0-degrees and back nozzles angle set at 30-degrees: a) flow rate vs pressure; and b) propulsion force vs. pressure.....59
Fig. 6. 2 – Results for six different single front nozzle diameters: a) flow rate vs. pressure; and b) backward force vs. pressure 60
Fig. 6. 3 – Results for different numbers of back nozzles only using the same 1 mm diameter for each orifice: a) flow rate vs. pressure; and b) propulsion force vs. pressure.....61

Fig. 6. 4 – Fig. 6.3 – Results for different diameters of back nozzles using two each of the same size and angle of 45-degrees: a) flow rate vs pressure; and b) propulsion force vs. pressure 62
Fig. 6. 5 – Results for various angles of back nozzles using two back nozzles with the same 1 mm diameter: a) flow rate vs pressure; and b) propulsion force vs. pressure....63
Fig. A. 1 – Results for Nozzle 1: a) flow rate vs. pressure; b) backward force vs. pressure 72
Fig. A. 2 – Results for Nozzle 2: a) flow rate vs. pressure; b) backward force vs. pressure.....72
Fig. A. 3 – Results for Nozzle 3: a) flow rate vs. pressure; b) backward force vs. pressure.....73
Fig. A. 4 – Results for Nozzle 5: a) flow rate vs. pressure; b) backward force vs. pressure 73
Fig. A. 5 – Results for Nozzle 7: a) flow rate vs. pressure; b) backward force vs. pressure.....74
Fig. A. 6 – Results for Nozzle 8: a) flow rate vs. pressure; b) backward force vs. pressure.....74
Fig. A. 7 – Results for Nozzle Combination 1: a) flow rate vs. pressure; b) propulsion force vs. pressure.....75
Fig. A. 8 – Results for Nozzle Combination 2: a) flow rate vs. pressure; b) propulsion force vs. pressure.....75
Fig. A. 9 – Results for Nozzle Combination 3: a) flow rate vs. pressure; b) propulsion force vs. pressure.....76

Abstract

Radial jet drilling (RJD) is a proven stimulation method to increase reservoir contact quickly and affordably while utilizing existing infrastructure and wellbores. RJD exploits a niche within the industry by targeting marginal reservoirs, thin pay zones, heavy oil reservoirs, coal bed methane, low-permeability reservoirs, and old, conventional, low-producing reservoirs. Development of the RJD technology has led to a multi-orifice nozzle, which generates a substantial cutting force (i.e. jet impact force) to penetrate the formation rock and a propulsion force to advance the bit into the formation. Only a handful of previous studies focus on modeling propulsion force to provide reasonable predictions. However, the models require empirically determined parameters to provide an accurate prediction of the propulsion force.

This thesis presents a generalized propulsion force model, based on mass, momentum, and energy conservation equations. The model utilizes the discharge coefficient for multi-orifice nozzles to determine the impact and propulsions force generated at each orifice. The predictions of the new model are compared with existing and new measurements and showed reasonable agreement. After validation, the model allows performing a parametric study for further optimization. The results of the parametric study presented extensively in the article can be a good reference for future nozzle designs and hydraulic force calculations for the RJD technology.

Chapter 1 – Introduction

1.1 Overview

The concept of radial jet drilling (RJD) has been around for decades now, and through advancements in technology, the technique has proven successful in different areas around the world. In short, radial jet drilling uses a high-pressure water jet to cut through rock, similar to the technology used to cut and engrave steel. The technique of RJD involves drilling of many small diameter laterals (micro diameter holes) from a single vertical wellbore to increase reservoir contact and consequently increase production **(Kohar and Gogoi 2014)**. The technique utilizes coiled tubing to convey the RJD system. These jet-drilled lateral holes bypass the skin zone and any near wellbore damage zone, encountering previously untouched hydrocarbon-bearing rock, creating a new conduit for reservoir fluids to flow **(Kohar and Gogoi 2014).**

Early-developed RJD systems use ultrashort radius curves (a 10 to 12-inch radius curve going from vertical to horizontal) to enter the formation. The systems utilize an erectable whipstock equipped with rollers and slides **(Dickinson and Dickinson 1985)**. These lessen the frictional forces and fatigue damage on the pipe when bending around the curve. The system operates between 8,000 and 10,000 psi water pressure to drill a 1.25-inch production tube and following the bit as it penetrates into the formation. With no cutting bit or drill string rotation, new methods are developed to drill the rock and advance forward. The technique requires a good understanding of the various hydraulic forces develop when RJD systems are applied including propulsion and jetting forces from the bit nozzles/orifices**.** In conventional drilling, either the bit, bit components, or the entire drill string rotates and the hydraulics design strives to optimize ROP (rate of

penetration), well integrity, cuttings removal, and borehole stability based on drilling cost **(Bin et al. 2016)**. Later, **Dickinson et al. (1992)** develop an improved ultra-short radius jet drilling system compatible with coiled tubing.

Through further refinement of the RJD technology, a smaller, more manageable system developed with a diverter, high-pressure fluid filter, high-pressure flexible hose, and the jet bit

(Buckman et al. 2013). The diverter coupled with the flexible hose allows a smooth entry around the 90-degree curve. When used on producing wells, commonly on rod pump, the pumping apparatus is removed, and the diverter is connected to the end of either straight tubing or coiled tubing and lowered to the desired depth. This system is less bulky, which enables operations in small casing sizes, even from wells drilled decades ago.

1.2 Problem Statement

Some studies (Li et al., Ruichang) developed hydraulic force models for radial jet drilling; however, the models make several simplifying assumptions that are not proven theoretically or justified experimentally. Moreover, they require experimentally determined parameters to provide accurate predictions. Without the aid of an accurate model, the RJD process poses more uncertainty that operators tend to shy away from, especially when working in marginal or depleted reservoirs. An accurate model allows determining working and pumping pressures and the subsequent flow rates throughout the operation. Hence, this study seeks to provide a generalized hydraulic force model for radial jet drilling, building upon established conservation laws.

1.3 Objectives

This investigative study looks into the hydraulic forces of the jetting nozzle in RJD. Previously developed force models require experimentally measured parameters to provide accurate predictions. Even though the outputs from the existing models can be replicated, some of the formulations of the models are unclear. The primary goal of this study is to develop an improved and generalized model. The specific objectives of this investigation include:

- Developing an understanding of the hydraulic forces at work with a jetting nozzle with emphasis on the hydraulic forces.
- Formulating a generalized force model to predict the propulsion force for multi-orifice nozzles.
- Investigating discharge coefficients of the jetting nozzle and developing a simplified correlation or model.
- Construct an experimental jet drilling set up to compare calculated and measured values to validate the mathematical model.
- Conduct a parametric study to determine the influence of various parameters.
- Compare published data with the developed model analyzing the differences from the experimental data acquired in this study.

1.4 Methodology

The approach for this research includes a literature survey, theoretical modeling, experimental investigation and theoretical analysis. The literature review provides the basic information needed for a fundamental understanding of RJD hydraulics and helps establish a foundation on the various intricate aspects of RJD. The theoretical and modeling parts of the investigation lead to the development of an improved model that accounts for different hydraulic related phenomena that are often considered negligible. The predictions of the new and existing models are compared with experimental measurements. This allows evaluating the accuracy of each model against the data acquired during experimental investigation and further assesses the validity of the dimensionless discharge coefficient correlation, developed in this study. The theoretical analysis looks into the influence of various parameters on the resultant forces in the system.

Chapter 2 – Literature Review

2.1 Application

With many conventional reservoirs nearing the limit of their primary production, a niche in the market came to fruition to recover more hydrocarbon from these formations. Many thought these conventional reservoirs were nearing their economic limit, but with the use of RJD, these fields can continue to produce with minimal time and capital. RJD incorporates various applications beyond just old, conventional reservoirs, these include, shallow, heavy oil reservoirs for injection methods, consolidated formations, coal bed methane (CBM), disposal wells, with some use offshore and mining practices **(Dickinson and Dickinson 1985)**. This creates an affordable method to stimulate shallow, marginal, low-permeability reservoirs efficiently in a short period of time (**Bin et al. 2016).**

In order to discuss the success of a technique or system, success requires some rigidity within the definition. In this study, success defined as any increase in production from a well after stimulating with RJD. Although, in some instances, increased production does not always indicate an increase in the rate of return. For example, a well can 'double' production, which sounds great, but if the well was initially producing 1bbl per day and the job cost was $100k, it would take almost three years to break even, not including operational costs to produce from the well. Many would deem these results unsuccessful from an economic standpoint. This also displays the common miscommunication when defining the success of an operation.

As for operating companies, economic benefit plays a significant role when determining success. The key considerations that make RJD an attractive stimulation technique are safety, cost, geological uncertainty, mobility, availability, environmental

risk, and time is. Safety is a priority throughout the industry, with minimal personnel and moving parts coupled with a short job time; RJD establishes a safer working environment. The geology becomes less of a factor due to the hydraulic forces of the jetting bit naturally keep the lateral in a horizontal plane and perpendicular to the central wellbore. The mobility of a coiled tubing unit appeals to operators working in tough terrain or remote areas. Availability plays a role because without a coiled tubing unit or proper RJD equipment, the job does not get off the ground. RJD significantly reduces environmental impact by creating a network of lateral holes using only water jet. This is a major benefit especially in areas where hydraulic fracking is outlawed. Fast and efficient operations are highly desirable, for any stimulation technique because time equates to money. Arguably, the most significant aspect, the cost can make or break any operation; however, with most coiled tubing working on a daily or hourly rate and job duration of roughly a day, time drives the cost for RJD operations.

Along with the major benefits aforementioned, RJD adds value to production. Jet drilling improves drainage efficiency through an increase in conductivity. RJD can enhance the mobility of high viscosity oils as well as create a conduit between multiple sweet spots and the central well. With a defined length and orientation of penetration into the formation, RJD helps better understand the near wellbore characteristics, which can lead to further experimentation. RJD also provides a solution to well intervention in environmentally sensitive areas, such as near-by aquifers **(Bruni et al. 2007)**.

2.2 Field Equipment and Procedure

Performing and RJD operation requires a few specialized tools and fittings to go along with a coiled tubing unit and sometimes a workover rig. The workover rig helps with pulling the production tubing from the well and setting the baffle anchor. The coiled tubing unit does not need any modification for tubing conveyed jet drilling, but in some instances, a specialized unit is used. One such specialize coiled tubing unit, used in Argentina, possessed **(Bruni et al. 2007)**:

- 13,500 ft of ½-inch pipe, with a maximum allowable working pressure of 10,000 psi,
- a motor to provide power,
- a triplex pump with a capacity of 2-5 bpm at 10,000 psi.
- an injector head to aid the pipe into the wellbore, and personnel to monitor the job

The bottom hole assembly (BHA) requires additional items to make RJD possible. When the job performed in Argentina, the additional item in the BHA was the tubing anchor. The purpose of the tubing anchor is to:

- Maintain the position of the tool when drilling through casing and into the formation
- Direct the tubing string smoothly around the short radius curve
- Prevent excessive torque when milling through casing

Two different BHAs were used in operation, one to penetrate or mill through the casing and another to drill into the formation. The penetration BHA includes **(Bruni et al. 2007):**

- 0.75-inch mill

- Locking nipple
- Elbow
- 1 11/16-inch motor

While the drilling BHA includes:

- Jet bit nozzle
- 328 feet of 0.5-inch Kevlar flexible hose

Depending on the situation and well, an RJD operation may need a workover rig to pull production tubing. The workover rig is set in place and well-conditioned before pulling production tubing. The depth of the formation calibrated with the equipment, followed by a pressure test of the casing to ensure no leaks. Flow rate and fluid samples of the targeted zone gathered to form an initial baseline for comparison of future production rates. With equipment set and preliminary data obtained, the anchor is lowered to the desired depth, and its position is verified with the casing collar locator (CCL) from wireline**.** The coiled tubing unit is mounted and assembled with the milling BHA to penetrate the casing**.** When the milling is completed, the tool is pulled, and the drilling BHA is assembled, followed by a second run in the hole while circulating at a moderate flow rate. When approaching the anchor, the flow rate is increased to slip the tool into the anchor and into the formation **(Bruni et al. 2007).**

2.3 Previous Studies

2.3.1 System Development

Like any other technology, RJD had to start somewhere, and the concept has been around for decades. Initially RJD started out relatively bulky and robust; however, through further studies coupled with trial and error, the system is refined to lower cost,

time, risk, and become more applicable and user-friendly. Early development targeted shallow heavy oil reservoir with multiple lateral holes at the same elevation **(Dickinson and Dickinson 1985)**. The lateral holes are drilled using RJD and equipped with a 1.25-inch production tube placed in each. These laterals could extend 100 – 200 ft through unconsolidated formations. The ultra-short radius concept comes from the 10 - 12-inch radius turn from vertical to horizontal in order to target thin pay zones and eliminating underreaming. What made the RJD possible is the development of the self-regulated propulsion system that works with internal fluid pressure. Fluid discharged through the front-facing nozzles creates a jetting force to cut the rock formation; however, its recoiling effect must be overcome by the backward facing nozzles to propel the bit forward. The propulsion forces also keep the hose and bit in tension, leading to a straight hole **(Dickinson and Dickinson 1985)**.

The development of an erectable whipstock coupled with internal rollers to reduce friction around the curve advanced the progress of the RJD technology. The whipstock shown in **Fig. 2.1** resembles an inverted question mark. It consists of a series of sliders and rollers to allow a progressive bending of the production tube **(Dickinson et al. 1986)**. The retrievable whipstock functions by first setting a downhole anchor, which is consisting of metal jaws that bite into the casing to hold the assembly in place. Then, by applying tension through raising the workstring about a foot sets the whipstock in place. By utilizing a gyroscope to determine the azimuth for each lateral, multiple laterals can be drilled within the pay zone and various layers may be drilled without bringing the whipstock all the way to surface**.** Also, note that 50-70% of RJD cuttings possess a diameter smaller than 1mm **(Chang 2006)**. Due to the low flow rates compared to

conventional drilling, most cuttings settle to the bottom, while larger cuttings flow back to the mother well and settle to the bottom of the vertical wellbore **(Bin et al. 2016)**. According to Bin et al. (2016), the vertical wellbore maintains the capacity sufficient to collect cuttings from and RJD operation. Another accolade in the development of RJD is the integration of the Control While Drilling (CWD) system (Fig. 2.2). The advancement of the CWD system required extensive research with many bumps along the way **(Dickinson et al. 1990).** The CWD consists of four side jets or nozzles 90-degrees from each other, monitored by an electric piloted, pressure valve switch. Axial motion is controlled by a motion controller (sealed piston) attached to the drillstring, which consists of seal and fluid orifices, similar to a shock absorber. The inclination is monitored using a real-time electromechanical inclinometer, which compensates for rolling of the bit by distributing the power with a set of solenoids. The four jets use flow-actuated valves, powered by high-pressure fluid.

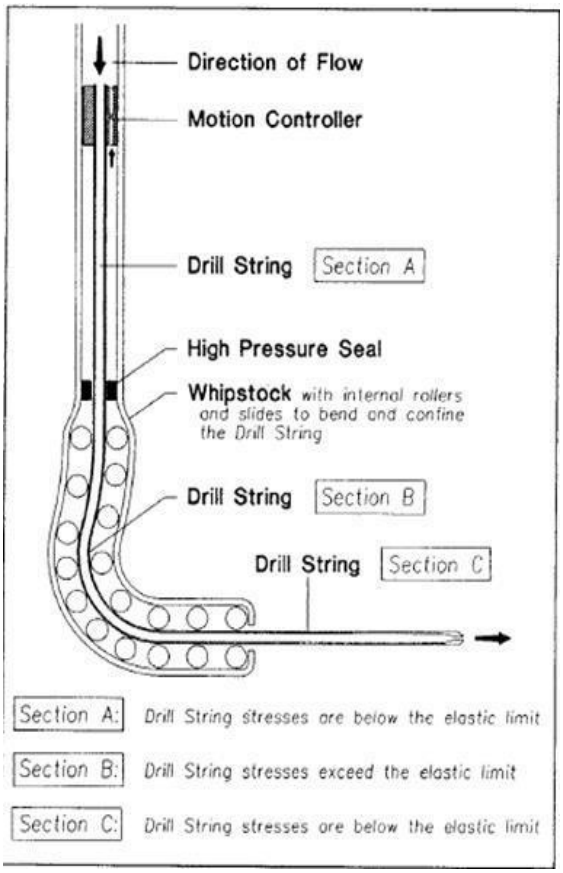

Fig. 2.1 – Schematic of the early RJD system (Dickinson et al. 1986)

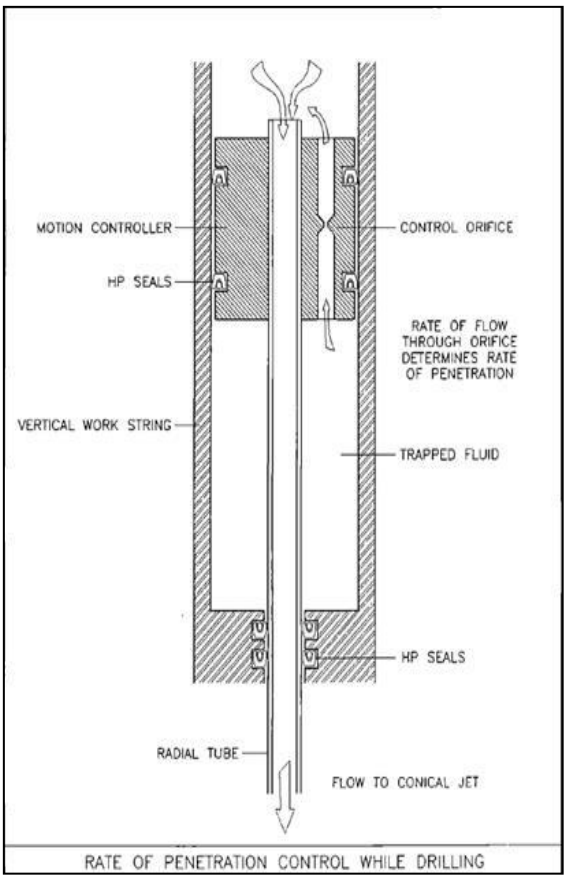

Fig. 2.2 – RJD control while drilling setup (Dickinson et al. 1990)

In order to simplify the RJD technique, the lateral hole diameter reduced from 4 to 1.5-inch and hose size reduce from 1.25 to 0.5-inch, putting less strain and fatigue on the pipe going around the curve. This also reduces the required flow rate to achieve the same operating pressures with a smaller diameter hose. The refined BHA consists of a tubing end connector, controller, anchor, Indexer, steering mechanism, and a stroke cylinder **(Buset et al. 2001)**. The tubing end connector, placed at the end of the coiled tubing allows simple connection to the BHA. The controller initiates tool functions, powered by a solenoid distribution system and a hydraulic power unit**.** The anchor also operates hydraulically, but it keeps the BHA in place to ensure the jet bit enters the hole milled into the casing. The Indexer helps in determining the orientation of the bit to

ensure the drilling of laterals that are perpendicular to the central vertical well. The Stroke Cylinder's function is to position the nozzle head in front of the casing hole (perforation).

Although similar to the old technique, which was developed 20 years ago, continued improvement on the system leads to the development of the RJD technology used today. From successful field operations, the Buckman Jet Drilling system **(Buckman et al. 2013)** consists of a coiled tubing unit, downhole filter, production tubing (already in place), diverter shoe, flexible hose, and the jetting bit displayed in **Fig. 2.3**.

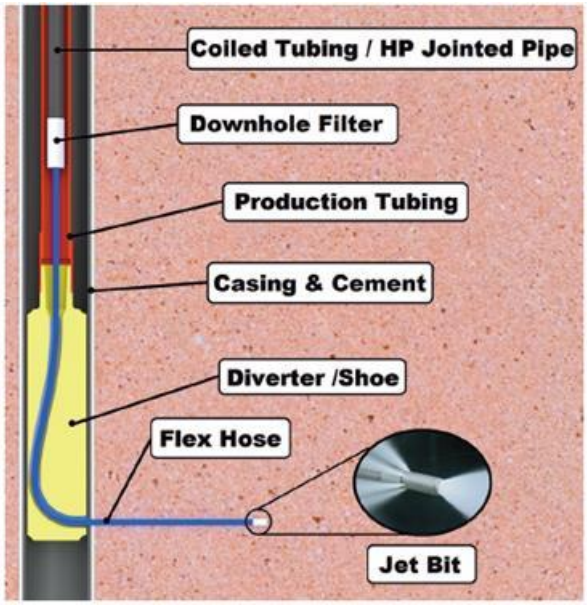

Fig. 2.3 – BHA of the Buckman Jet Drilling system (Buckman et al. 2013)

The key upgrades to the Buckman system include the jet bit and the flexible hose. The jetting nozzle is a 1-inch diameter consisting of 5-6 backward facing nozzle with 1-3 forward facing nozzles. The flexible hose is a braided hose made from either Kevlar or material similar to Kevlar to ensure strength and maintain pressure capabilities **(Bruni et al. 2007)**. One interesting aspect of the Buckman setup is the use of their 'Flatpak,' where a dual-coiled tubing strings ran at the same time (one string inside the other), permitting underbalanced drilling.

2.3.2 Field Studies

The question many in the industry care about is the system and its field applicability. The concept may be great theoretically; however, nearly impossible to perform. For the industry, success is determined from the results in the field. The RJD technology has demonstrated many successful field cases on the production enhancements from around the world including the United States, Argentina, China and Egypt to name a few. There have been a number of studies (Bin et al. 2016, Bruni et al. 2007, Buckman et al. 2013, Cinelli and Kamel 2013, Kohar and Gogoi 2014, Ragab and Kamel 2013) showing a surprising level of success in terms of productivity improvement, but none includes the Rate of Return (ROR) for the operator or the break-even time. Although estimating prices and costs can suffice a general study, further individualized pricing would help to determine the economic benefit of using RJD as opposed to another enhanced oil recovery or completion technique.

A field study conducted in the La Barge Field in Wyoming consisted of eight different wells, six offset vertical wells without intervention, one well before and after drilling three radials, and one new well drilled with three radials **(Dickinson et al. 1993)**. The data in **Fig. 2.4** displays the range of oil production rate for wells with and without RJD intervention, with the wells on the left being only vertical wells and the wells on the right being wells that were jet drilled. **Table 2.1** provides the decline rate for water and oil to give an understanding of the initial production before any RJD operation**.** According to the data, the reentry of well J634 drilled three radials with lengths 54 to 70 ft exhibited an increased production in oil of about two times and reduced declination rate by about half. The expectation of a larger production increase lead to the assumption that wellbore damage was not as severe as expected. The production increase of the new well

G634y with three radials roughly four times compared to the offset vertical wells. In this case, the production bump assumed to be from penetrating through the skin or damaged zone near the wellbore into more virgin rock. From this study, RJD seems acceptable, but with only two wells jet drilled there is not enough data for a definitive stance on RJD operation. The scope of this study does not encompass the economics before and after an RJD job, production may increase, but if the well takes several years to break even, this would not be good from an operator's standpoint.

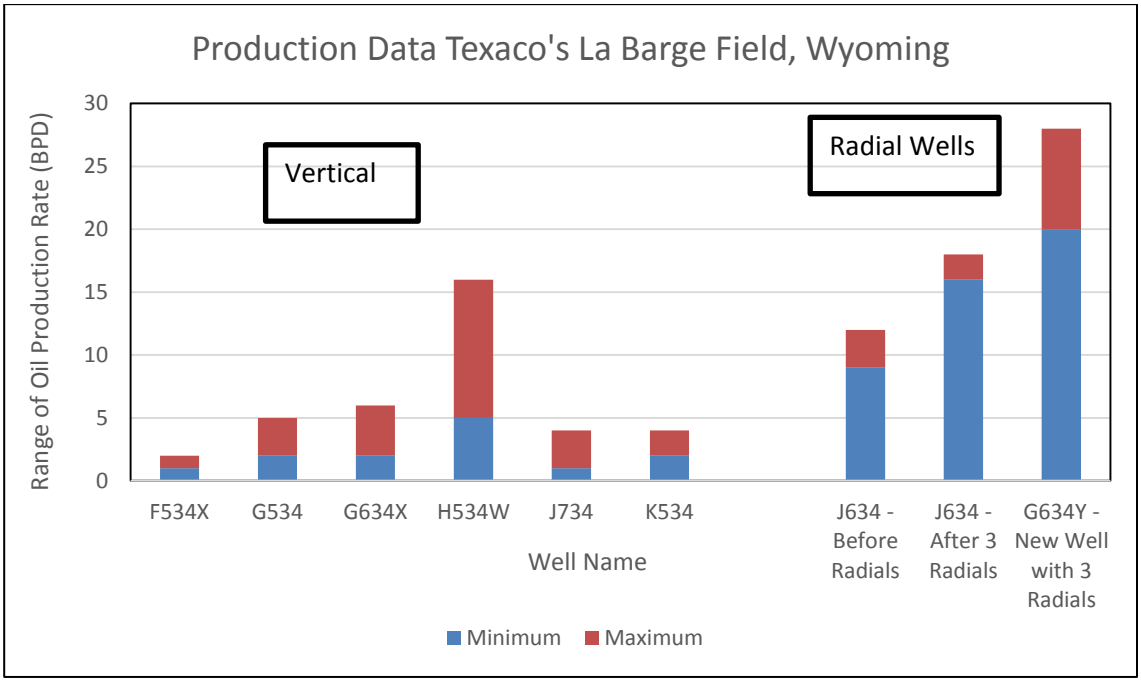

Fig. 2.4 – Oil Production rate with and without RJD (data from Dickinson et al. 1993)

A study from the Liaohe Oilfield in China in 1999, in which four radial boreholes drilled at three different depths, noticed increases in production up to 400% **(Yonghe et al. 2000)**. Unlike the initial case, the RJD operation was followed by hydraulic fracturing and gravel pack completion. By hydraulically fracturing the well after jet drilling, this significantly increased the cost of the operation to roughly $1 million. Although, cheap in comparison to the plug and perf technique used today, this is far too expensive when

the niche is extending the life or enhancing production of depleted or thin pay zones. This also poses the question, what influenced the increase in production? Was it the hydraulic fracturing, the jet drilled laterals, or some combination? For better comparison, keeping the RJD well intervention process as consistent as possible is key.

Table 2.1 – Oil and water production rate with and without RJD intervention

Well	Water Production	Oil Production Decline Rate
F534X	Nearly Clean	
G534	Declining from 200 bwpd to 36 bwpd	
G634X	Declining from 160 bwpd to 25 bwpd	
H534W	Fluctuating from 1 bwpd to 2 bwpd	
J734	Fluctuating from 10 bwpd to 100 bwpd	
K534	Fluctuating from 30 bwpd to 80 bwpd	
J634 - Before Radials	Fluctuating from 2 bwpd to 5 bwpd	Declining 63% over 10 months
J634 - After 3 Radials	Nearly Clean	Declining 33% over 18 months
G634Y - New Well with 3 Radials	Increasing to 7 bwpd	Declining 49% over 18 months

A study conducted in Argentina from Golfo San Jorge and the Neuquén basins obtained conflicting and inconclusive results **(Bruni et al. 2007)**. Several factors with varying degrees of uncertainty all played a part including: basin, formation, fluid type, depth, production rate, formation damage or skin, bit orientation, and drilling direction. With this many ambiguous elements, it is hard to obtain definitive results, but this study is imperative for the RJD technology learning curve. From the study, the operations for the shallower wells went a bit smoother than the deeper wells. A major issue encountered was determining the orientation of the lateral holes and the direction of the jet bit while drilling. This coupled with using production rate as the control creates a lack of consistency amongst test wells. Production as control works well with little uncertainty, but the wells tested targeted various pay zones and some multiple zones in a single well. Although production may have increased, it could have been from a single formation,

testing various zones at once only added to the uncertainty. Along with the shallow wells that yielded increased production, so did one of the heavy oil wells, which initially was unproductive. These are promising results, but the data needs to be approached with a bit of skepticism due to the high level of uncertainty.

A similar study conducted in Egypt from the Belayim Oil Field, in which three tests wells were drilled with multiple laterals **(Ragab and Kamel 2013)**. At depths between 7,100 and 8,100 ft, seven laterals drilled in Well 1, six laterals in two separate zones for Well 2, and the third well (Well 3) with four laterals drilled. From a mechanical and operational standpoint, the RJD application succeeded in drilling multiple laterals in a single wellbore. From a production point of view, oil production increase from 12% - 47% in the tested wells, but a couple of issues with this study are the duration of the production increase and the initial rate. The increased production eventually tails off, but the purpose is to either get as much oil out of the ground as soon as possible or decrease the slope of the decline curve. Another observation was production increased with lateral length in Well 2, some of the laterals were drilled to almost 300 ft while the rest were drilled to a length of 165 ft. This study offers improvement from the previous study in Argentina; with a reduction in uncertainty, it is easier to analyze pre and post RJD production data.

A field study (Cinelli and Kamel 2013) conducted in Cowley County, Kansas, provides near ideal conditions for the specialized RJD technology. The marginal Donelson West field and the carbonate formation produced via the primary gas drive since 1967 up until this study took place. Porosity varied between 15 - 20%, permeability 1 - 10 md, and pay thickness from 6 – 10 ft, this renders current horizontal drilling and completion

techniques uneconomical. The main difference between this study and the two previously mentioned (Ragab and Kamel 2013; Bruni et al. 2007) is the use of acid during the completion process. Being a limestone formation, the acid helps dissolve the calcium carbonate allowing for faster drilling and little concern with cuttings. The redevelopment of this older field consisted of the intervention of eight existing wells and drilling two new wells. Along with drilling multiple laterals, each well was hydraulically fractured using acid and nitrogen. Table 2.2 provides production data before and after the RJD operation with the Pre-RJD data being the field's total monthly production and the Post-RJD data being the nine months following the operation. The data indicates a significant production increase for the field as well as the older wells for at least nine months. Although this operation deemed a success, the question arises; to what impact did RJD provide? Was the production increase influenced more by the acid frac or RJD? This study is beneficial to the progression of the RJD technology, but performing the acid frac adds to the uncertainty of the data. This is understandable because operators are in the business of making profits and less about experimentation.

Similar to the study in Kansas, data provided by Buckman Jet Drilling (**Buckman et al. 2013**) gives a little insight on the production enhancement, formation depth, number of laterals drilled, and the average penetration of those laterals. The benefit of this data allows for a better understand applicable depths for RJD, increased reservoir contact, and the improvement in production. For proprietary purposes, all well names have been removed. **Table 2.3** displays two systems of RJD data, one using a KOS Energy (now Petrobore Energy) system and the other a Sheath system (**Buckman et al. 2013**). The number of laterals ranges from 8 to 16 with average penetration ranging from 4 to 40 ft.

The commonality amongst these wells is the uptick in hydrocarbon production, but operational differences pose uncertainty within the results. The results are encouraging; nevertheless, again it is difficult to call the operation a success with such low production rates and the lack of financial data.

Table 2.2 – Production data before and after RJD (data from Cinelli and Kamel 2013)

Pre-RJD		Post-RJD			
			Total Monthly Field Production	Old wells total monthly field production	Average monthly production per well
Year	bbl/month	Months after	bbl/month	bbl/month	bbl/month
2002	11	1	1100	231	33
2003	62	2	974	244	35
2004	125	3	976	234	33
2005	106	4	961	248	35
2006	85	5	789	221	32
2007	70	6	790	213	30
2008	133	7	1124	475	68
2009	142	8	797	247	35
2010	197	9	803	265	38
Average ('08-'10)	157	Average	924	264	38

Table 2.3 – Pre and Post RJD production data (courtesy of Dr. Buckman with BJD)

Depth (feet)	Average Penetration (feet)	# of Laterals	bopd Pre SRS	bopd Post SRS tot	Pre/Post
1750	40	12	1	20	2000%
1240	30	16	5 mcfd	80 mcfd / 2 bopd	1600%
337	4	12	0	2 bopd	>200%
730	12	12	0	20 bopd / fracture	>200%
1310	12	16	0	14 bopd	>1000%
1200	20	16	0	12 bopd	>1000%
1200	14	16	0	3 bopd	>200%
1310	20	16	0	2 bopd	>200%
Sheath System					
1237	20	8	1	3 bopd	300%
780	15	8	0.75	2.75	360%
1035-1038	15	8	0.5	1	100%
1150	15	8	0.25	0.5	100%
748	12	8	1.5	0.5	30%
1240	12	15	0.25	2.75	900%
1755-1759	16	8	2.5	3 3/4	100%
1740-1744	16	8	2.5	3 3/4	100%

The aforementioned production studies all have one thing in common, increase or extend the economic life of a well or reservoir. Although the concept and implementation remain similar throughout, they lack scientifically acceptable assessment methodology, which leaves no doubt on the performance of RJD. On the other hand, it is difficult to conduct accurate field studies leading to a definitive result. Unknown or unproven technology often leaves people hesitant, because one mistake can cost thousands or even millions of dollars. The cost of conducting a field study also deters some from trying RJD; this demonstrates the necessity of experimental and theoretical investigations.

2.3.3 Theoretical Studies

Extending the life of a well or reservoir through RJD looks into two main factors, cost and efficacy. Cost is set through industry supply and demand, which often varies; however, it is out of the control of the operator, while efficiency continues to improve due to research and experimentation. The purpose of many theoretical RJD studies is to either enhance or question material on the subject. RJD incorporates many fine details

that would otherwise go overlooked. However minute, there is always room for improvement, and this is what theoretical studies seek.

RJD utilizes high-pressure fluid to penetrate into the rock formation. Bruni et al. identified four different mechanisms of penetration: surface erosion, hydraulic fracturing, poroelastic tensile failure, and cavitation (**Ragab and Kamel 2013**). Surface erosion denotes the process of fragmenting the rock surface due to the compressional and shear forces, applied by the jetting force. Hydraulic fracturing is the failure of the formation due to pressure change. An immediate drop in fluid pressure at the surface of a rock induces tensile stress in the formation. The stress is related to the reduction in pressure. When the induced tension becomes greater than the effective stress of the formation, the rock begins to fail. As the rock grain compressibility and pore fluid become imbalanced, tension induces, and the rock can only equilibrate from fluid migrating through pore space. Cavitation occurs when vapor bubbles implode or collapse on the surface of the formation causing shock waves.

One study **(Chi et al. 2015)** examined the maximum drillable length of RJD and developed a method to predict this length. This study observed a recoil force from the forward facing nozzles due to the high exit velocity of the fluid. With the backward facing nozzles being the only force propelling the bit forward, researchers observed a linear increase in friction with fluid pressure within the flexible hose. Flow rate dominates ROP during drilling, while maximum lateral length decreases with an increase in friction coefficient. To achieve the maximum drilled length, there is an optimum range of flow rate ratio (i.e. flow rate through forward facing nozzles to flow rate through

backward facing nozzles) around 0.2 - 0.3. The model developed helps to estimate the maximum drillable lateral length.

Another RJD study **(Chi et al. 2016)**, investigated the effects of various parameters of a multi-orifice jetting nozzle, which include, the rock breaking capacity and propulsion force. The number of orifices, orifice diameter, and inclination angle were examined to determine an optimal arrangement for each. As reported by **Chi et al. (2015),** an increase in the equivalent diameter and a decrease in inclination angle, improved the rock breaking efficiency. The equivalent diameter is determined from the whole section area of the front or backward orifices. Where d_e denotes equivalent diameter and the subscripts *f* and *b* signify either forward or backward direction of the orifices.

$$d_{ef} = \sqrt{n_f d_f^2} \tag{2.1}$$

$$d_e = \sqrt{n_f d_f^2 + n_b d_b^2} \tag{2.2}$$

The optimum number of orifices found to be six to seven with the optimum angle of inclination ranging between 12.5° and 22.5°. This study also indicated that an increase in the diameter and number of backward orifices and decrease in the angle of inclination resulted in an increased propulsion force.

Continuing on the subject of orifices, a variety of studies look into the numerous parameters to understand the effects of each including pressure drop, aspect ratio (L/d), diameter ratio (β = d/D), Reynolds number, shape, flow patterns. Johansen (1930) conducted a study to analyze the flow characteristics of sharp-edged orifices to determine

the discharge coefficient of orifices with five difference diameter ratios at 0.009, 0.209, 0.401, 0.595, and 0.794, with Reynolds numbers up to 25,000, using three different fluids, Castor oil, mineral oil, and water. Johansen noted that an increase in the diameter ratio leads to a higher Reynolds number at which the flow transitions come about, meaning the flow remains laminar for increased diameter ratios at higher Reynolds numbers.

Another experiment conducted by Medaugh and Johnson (1940) studied the pressure drops across brass orifices. Medaugh and Johnson made two key observations, one, that as flow rate through an orifice increased, the discharge coefficient decreased, and two, that as the diameter of the orifice increased, the discharge coefficient decreased for the same pressure drop. The authors concluded that the discharge coefficient would eventually decrease to 0.588 if the flow rate increased enough, but this value is roughly 6% less than data from Smith and Walker (1923) often used at the time. The potential issues regarding the Smith and Walker data are possible bowing of the plate due to high pressures, or a possible depression around the orifice when drilling the hole.

The next couple of studies examined cavitation and the effects on discharge coefficient. Kim et al. (1997) tested three orifices with diameter ratios of 0.10, 0.15, and 0.33, to look into the effects that plate thickness and cavitation have on discharge coefficient. For each respective diameter ratio cavitation appeared for β=0.10 with Reynolds number above 14,000, for β=0.15 with Reynolds number above 43,000, and for β=0.33 with Reynolds number above 100,000. Kim et al. noticed cavitation had no effect on the discharge coefficient for the diameter ratios used with a 0.55 aspect ratio or less over the range of Reynolds numbers examined from 4,000 to 170,000.

Ramamurthi and Nadakumar (1999) investigated square-edged orifices and the effects of cavitation and aspect ratio on discharge coefficients. Using aspect ratios from 1 to 50 with orifice diameters of 0.3, 0.5, 1.0, and 2.0 mm and tested at fluid rates with Reynolds numbers from 2,000 to 100,000. The study discovered that as cavitation appeared in a flowing fluid or the flow became separated that orifice diameter was the only function of discharge coefficient, while flow without cavitation both Reynolds number and aspect ratio affected the discharge coefficient. Noted in the flow region with cavitation that discharge coefficient increased with a decrease in orifice diameter. Ramamurthi and Nadakumar proposed that the increase in discharge coefficient stems from an increased wetting of the orifice walls and surface tension induced pressures. The study also found augmented disruptions in the fluid jet when flow is cavitating for orifices with an aspect ratio around five. Ramamurthi and Nadakumar noted this is probably due to cavitation bubble imploding near the orifice exit.

Chapter 3 – Theoretical RJD

3.1 RJD Force Theory

Numerous forces influence the performance of the RJD bit nozzle, which fall under either the cutting forces or the propulsion forces. The cutting forces are generated from the high-pressure discharge of fluid from an array of the front or forward facing nozzles or orifices **(Dickinson and Dickinson 1985)**. These nozzles (**Fig. 3.1**) are considered to act as small diameter orifices. Relevant operational factors to consider is the discharge coefficient when fluid flowing from a relatively larger diameter to a small diameter as well as its erosional effects on the bit. The high-velocity fluid erodes the nozzle outlet and increases its diameter, thus reduces the cutting force. The propulsion force, like the cutting force, also generated from the high-pressure discharge of fluid from an array of the backward facing nozzles (orifices).

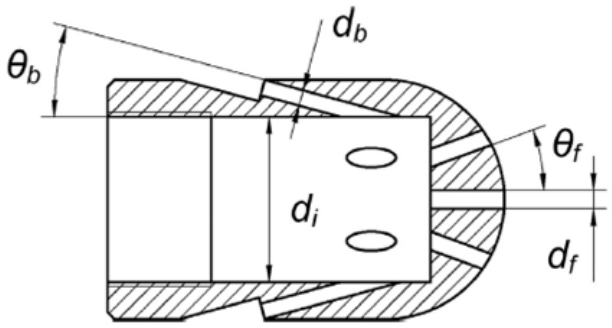

Fig. 3.1 - Design of RJD bit (Bin et al. 2016)

Optimization of the cutting force incorporates many factors, such as number of nozzles, nozzle diameter, inclination angle, fluid velocity, pressure differential, and discharge coefficient. Many of these factors apply to the propulsion force as well. The cutting force must be large enough to penetrate into the rock formation; however, it should be less than the propulsion force. Otherwise, the bit cannot advance into the

formation. Previous studies have indicated an optimal number of front-facing orifices and angle of inclination. Simply, more nozzles easy penetration into the rock, but the angle of inclination cannot be too large; otherwise, this hinders the cutting capability. Nozzle diameter influences the fluid discharge velocity; the decrease in front facing nozzle diameter increases the fluid velocity and consequently recoiling effect of the jetting bit. Under ideal conditions (frictionless), discharge coefficient equals one, meaning the theoretical flow rate is equal to the observed flow rate. However, the flow through the nozzle is not frictionless. This condition makes the discharge coefficient challenging to predict and model accurately.

These same concepts apply to the propulsion force in a similar fashion, but the key difference is the propulsion force must move the bit forward while overcoming the cutting force, tension force of the hose, and mechanical frictional forces. The propulsion force also influences the direction of the bit, optimally the bit maintains a straight path; however, an imbalance of propulsion to cutting force can cause the bit to sag and drill downwards or climb drilling upwards through the formation. Maintaining the bit on a straight path reduces friction with the formation and allows longer drilled laterals.

3.2 Existing Models

A common practice of comparing theoretical results with available experimental data helps formulate a model. RJD hydraulic models can be highly beneficial by setting a theoretical baseline or control as a reference point to compare and interpret experimental or field data. A quote from the statistician George Box states, "All models are wrong, but some are useful," meaning that models are based on assumptions that may or may not be applicable to a particular case. Models have limitations; thus, it is imperative to

approach any model with a slight amount of skepticism. This section discusses two theoretical models regarding the propulsion or pulling force of the jetting bit. Both models, replicated from literature, present advantages and disadvantages, touched on later in the section.

3.2.1 Theoretical Model 1

A study conducted by Ruichang et al. (2009) established a mechanistic model for the jet bit and high-pressure hose as well as analyses of what was termed the "hydroseal" or "depression effect" from the backward jets and the axial force distribution. The "depression effect" defined as the steady low-pressure zone which acts as a seal from the high-speed water ejected from the backward nozzles that mix with fluids in the annulus and carrying these fluids backward.. With the drilling system specifically containing backward facing nozzles, the type of jet bit generate both forward and backward jets. The forward nozzles arrange with multiple jets or in a swirling pattern, used to cut and break the rock. The backward jets function to pull the bit and increase hole size while simultaneously removing cuttings. Based on momentum balance, Ruichang et al. (2009) expressed the pulling force represented as:

$$F_{drag} = P_{in}A_{in} - P_{out}A_{out} - \rho Q_{front}\left(v_{front} - v_{in}\right) + n\rho Q_{back}(v_{back}\cos\theta + v_{in}) \quad (3.1)$$

where P_{in} and P_{out} indicate the inlet and outlet pressures of the jet bit (**Fig. 3.2**). A_{in} and A_{out} are the inner and outer sectional areas of the bit. Q_{in} and Q_{out} are the flow rates of the forward and backward jets. V_{front} and V_{back} are the flow velocities of the forward and backward jets, with v_{in} being the flow rate in the hose, and θ is the angle between the axis

of the backward nozzles and the jet bit. The first two terms on the right side of Eq. (3.1) represent forces generated by the inlet and outlet pressures and the last two terms represent the momentum fluxes entering and leaving the control volume. Note the equation shows that as the angle θ decreases, the pulling force increases, with a maximum at angle equal to zero. The flow rate of the bit is limited because the jets must be capable of breaking the rock. Thus, the flow rate of the backward jets cannot increase infinitely and the pulling force due to momentum exchange cannot be too large. The high inner pressure primarily drives the pulling force of the jet bit.

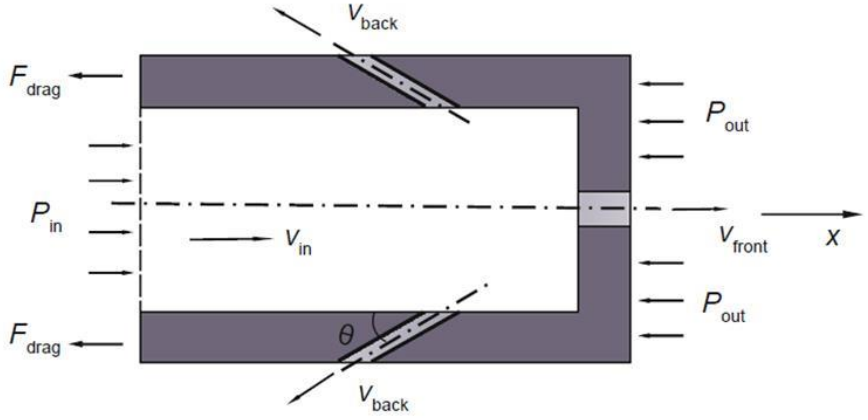

Fig. 3.2 – Simple nozzle illustration of the forces in the system (Ruichang et al. 2009)

When the forward nozzle is located at the center of the jet bit, the resultant force in the radial direction is zero due to the symmetrical arrangement of backward nozzles, resulting in improved stability of the jet bit and high-pressure hose. The force analysis of the high-pressure hose, simplified by assuming one-dimensional horizontal forces in the x-direction yields the following equation:

$$P_1 A_1 + F_{pull} = P_2 A_2 + F_{drag} + F_f \tag{3.2}$$

where F_{pull} and F_{drag} are the corresponding forces acting on the hose in the forward and backward direction. P_1 and P_2 are the pressure in the forward and backward directions, and A_1 and A_2 are the flow cross-sectional areas of the inlet and outlet of the high-pressure hose. Pressure drop is primarily due to hydraulic friction along the hose in the x-direction. Thus:

$$F_{drag} = F_{pull} - F_f + P_1A_1 - P_2A_2 = F_{pull} - F_f + \frac{2f\rho v_0^2 L}{d} \quad (3.3)$$

The frictional coefficient is denoted as f, v_o is the flow velocity in the high-pressure hose, L is the length of the hose, and d is the inner diameter of the hose. The mechanical friction (F_f) between the hole wall and the high-pressure hose, expressed as:

$$F_f = \mu K_b q_p L \quad (3.4)$$

Here, μ denotes the frictional coefficient between the high-pressure hose and the hole wall, K_b the buoyancy factor, and q_p is the weight of the hose per unit length. The weight of the hose per unit length is quite small and consequently so is the drag friction between the hole wall and high-pressure hose. The pressure drop along the hose generates thrust, positive in the x-direction, so the drag force, equal to the pulling force of the next hose segment, shows little decrease with an increased length of the hose. This keeps the hose in tension allowing the bit to extend into the formation in a straight and steady path.

Mentioned in this study, the 'depression effect' of backward jets, defined as the steady low-pressure zone which acts as a seal from the high-speed water ejected from the backward nozzles that mix with fluids in the annulus and carrying these fluids backward. This seal can reduce the chip hold-down effect to increase penetration and decrease backward pushing force generated by the pressure downhole which increases the relative

pulling force. To calculate the pulling force, the differential pressure coefficient (β) is introduced as:

$$\beta = \frac{(P_0 - P_{out})}{Q} = \frac{\Delta P}{Q} = f(Q, D) \tag{3.5}$$

With P_0 as the annular pressure behind the jet bit, Q as the total flow rate, and D as the hole diameter. β represents the ability to generate this low pressure zone, but also difficult to calculate due to the complexity of downhole flow fields. The pressure in the front of the jet bit shown as:

$$P_{out} = P_0 - \beta Q \tag{3.6}$$

Combining Eqns. (3.1) and (3.6), the pulling force of the jet bit is calculated by:

$$F_{drag} = P_{in}A_{in} - (P_0 - \beta Q)A_{out} - \rho Q_{front}\left(v_{front} - v_{in}\right) + n\rho Q_{back}(v_{back}\cos\theta + v_{in}) \tag{3.7}$$

The experiments were conducted to investigate the pressure drop across the jet bit, annular pressure loss, and pulling force acting on the jet bit in different hole diameters. The set up used a bit with a single forward jet, operated at flow rates between 0.1 - 2.0 L/s, in hole sizes of 30, 40, and 50 mm . The equipment schematic illustrated in Fig. 3.3 shows the power system, circulating system, experimental device, and data acquisition system used in the study.

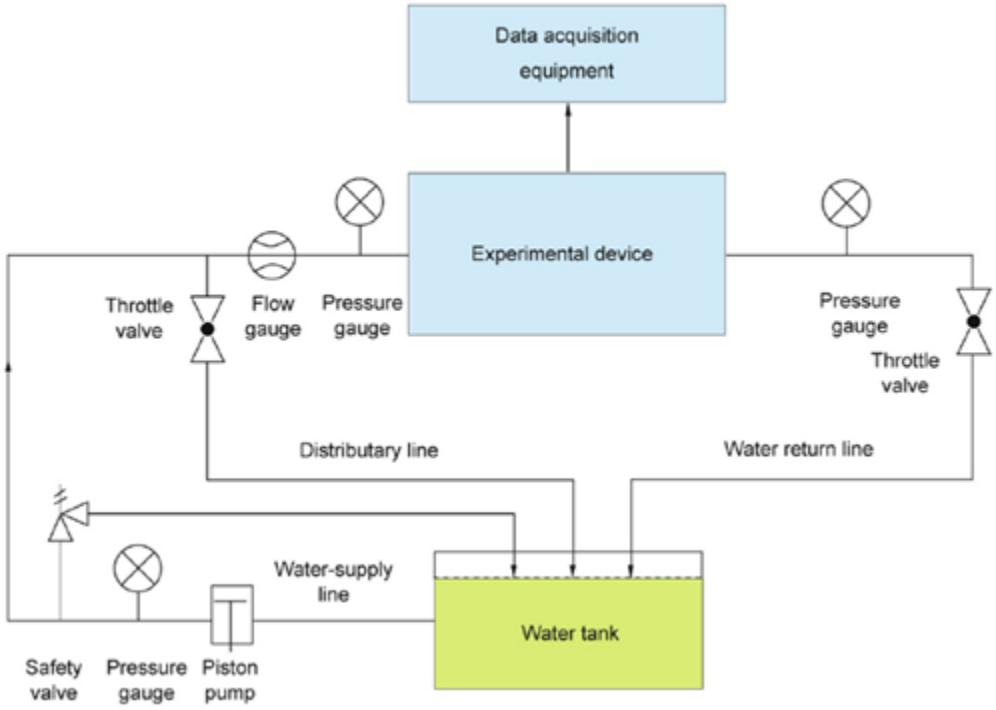

Fig. 3.3 – Schematic of the experimental setup (Ruichang et al. 2009)

Fig. 3.4 depicts a parabolic relation between pressure drop and flow rate, with a higher flow rate indicating an increased pressure drop. The experimental results are nearly identical to the theoretical calculation. The primary driver of the pulling force is the pressure inside of the jet bit. Meaning, the flow rate must be sufficient for the bit to produce enough pull force**.** Ruichang et al. (2009) presented the differential pressure coefficient as a function of the flow rate for various hole diameters **(Fig. 3.5)**. The trend of the coefficient is approximately linear increase with flow rate and a large hole reduces the slope of the line.

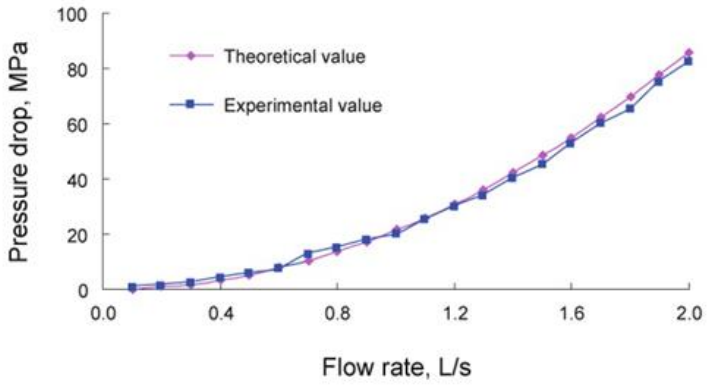

Fig. 3.4 –Pressure drop vs. flow rate (Ruichang et al. 2009)

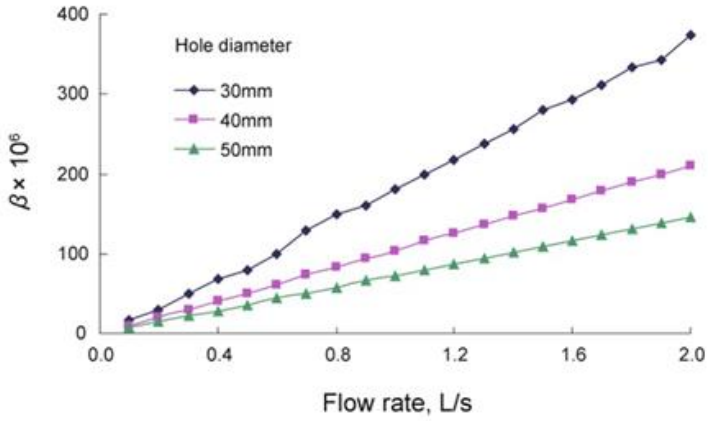

Fig. 3.5 – The differential pressure coefficient vs. flow rate (Ruichang et al. 2009)

The relation between flow rate and the pulling force of the jet bit in different hole sizes is shown in **Fig. 3.6**. The trend depicts a parabolic relationship with experimental values nearly identical to the theoretical values, within 3% margin. Pulling force remained low at flow rates around 0.5 L/s, but significantly increased at flow rates over 1.0 L/s with a maximum force of 8,000 N at a flow of 2.0 L/s .

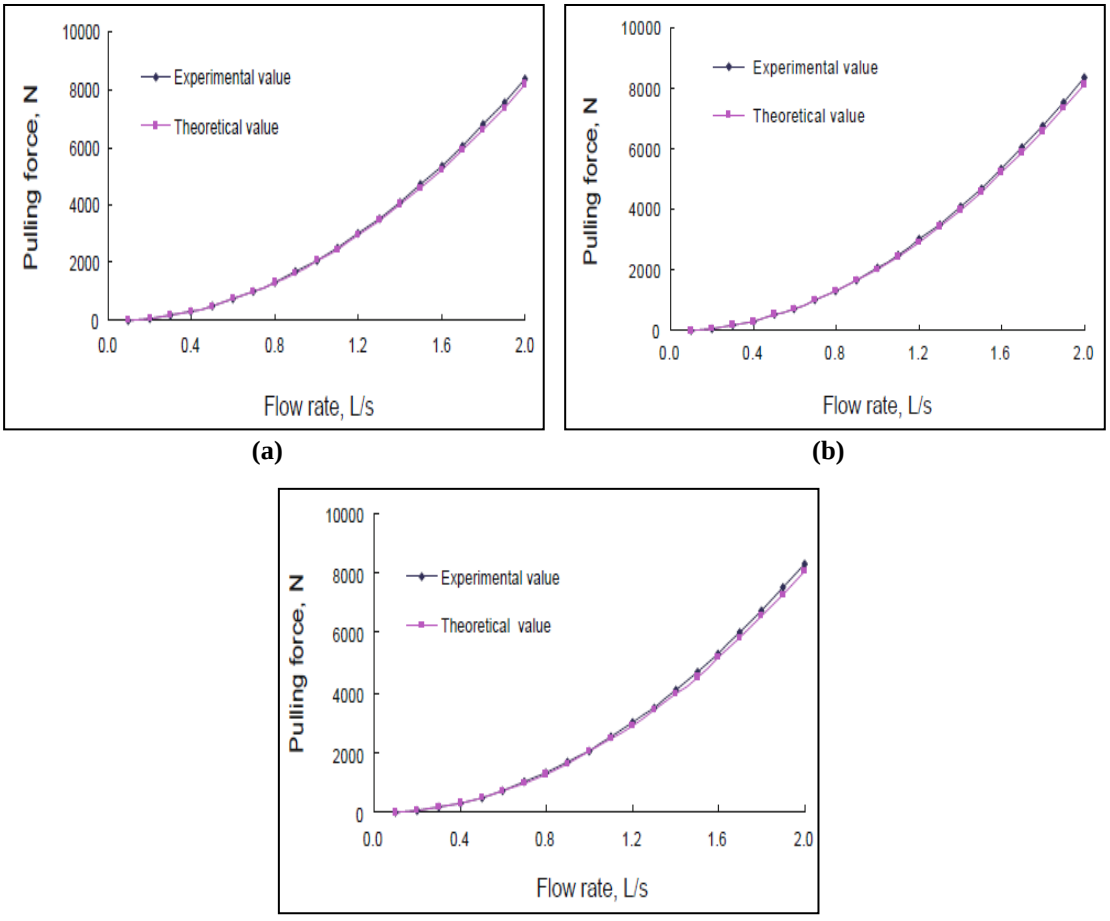

Fig. 3.6 - Pulling force vs. flow rate for different hole sizes: a) 30mm; b) 40mm; and c) 50mm

Examining the effect of hole size on the pulling force using the model shows the negligible impact of the hole size. The plots in Fig. 3.6 show model predicted pulling force versus flow rate for 30 and 50 mm diameter holes. There is little to no difference between the values of 30-mm and 50-mm holes, verifying the minor effect of holes size on the pulling force.

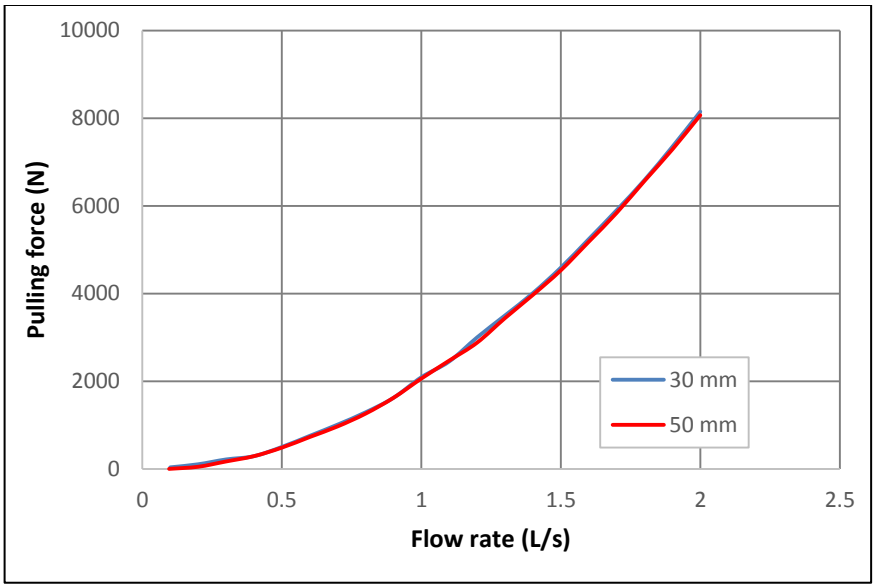

Fig. 3.7 – Model predicted pulling force vs. flow rate for different hole sizes

This model posed a bit more difficulty trying to replicate due to the limited data provided in the paper. The scope focused more on differential pressure coefficient and testing different hole diameters for flow rate versus pulling force. By using the plots provided in the paper to replicate the data and a digitizing software, provides a reproduction of the plots. The digitizing software "Digitize It" worked to only three significant figures, thus providing only estimations of the data. The output values from this model appear significantly larger than the other model, especially as flow rate increases. Hypothetically speaking, this model may overestimate propulsion force, but provides another reference point for comparison later on.

3.2.2 Theoretical Model 2

The second model to discuss has been developed by Li et al. (2015). It is originated from a study that was focused on the self-propelled forces of a multi-orifice nozzle. The model calculates the self-propelled force and defines a factor to signify self-

propulsion ability of the nozzles. The self-propelled force is defined as the force generated by the nozzle to push the bit forward. The multi-orifice bit nozzles are divided into two groups: the forward and backward orifices/nozzles. The forward orifices generate the impact force from high-pressure fluid to break the rock, while the backward orifices produce the self-propelling force along with tendency of expanding the hole. The jetting nozzle operates as the engine for RJD. Subsequently, it is essential to analyze its rock breaking characteristics. Only a few studies provide a model for the self-propelled force of a multi-orifice nozzle. Li et al. (2015) developed a model and validated by experimentation. The study looked into the impact of the various jet bit design and operational parameters on the propulsion force. Fig. 3.8 shows a simplified two-dimensional illustration of the multi-orifice nozzle.

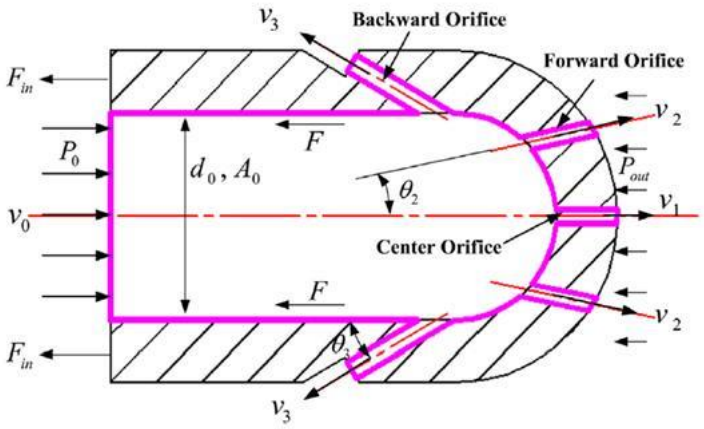

Fig. 3.8 – Design of a multi-orifice nozzle (Li et al. 2015)

The nozzle configuration consists of n_1 forward orifices at the center, n_2 forward orifices, and n_3 backward orifices. The corresponding diameters, velocities, and flow rates include d_1, d_2, and d_3; v_1, v_2, and v_3; and Q_1, Q_2, and Q_3. The angles between the center axis and nozzles are θ_1 and θ_2 with the hole diameter as d_o. The incoming flow rate, velocity, and pressure are Q_o, v_o, and P_o, respectively. The pressure at the orifice

discharge labeled p_{out}, and F_{in} is the mechanical contact force applied to the nozzle by the high-pressure hose. The self-propelled force denoted as *Fsp*, while *F* is net force. The model is developed based on the following fundamental assumptions:

- The working fluid is incompressible.
- The velocity of the fluid at each orifice is equal to the average velocity.
- The flow is steady.
- The bit is oriented horizontal; hence, the force of gravity is not considered.

According to the model, the net force applied on the bit is equal to the sum of the contact force F_{in}, the self-propelled force F_{sp}, and the shear stresses, which are often small and therefore neglected. Then, the net force is expressed as:

$$F = F_{in} + F_{sp} \tag{3.8}$$

This study only considers the axial momentum equation due to the symmetrical structure and arrangement of orifices on the nozzle. It assumes for a specific case that the diameters of all forward orifices are the same, and consequently so are the flow rates. Based on these assumptions the self-propelled force expressed as:

$$F_{sp} = \frac{\rho}{A_0} m Q_0^2 \tag{3.9}$$

where ρ is fluid density in kg/m^3, A_0 is the cross-sectional area of the nozzle in mm^2, Q_0 is the incoming flow rate in L/s, m is the self-propelling dimensionless factor of the nozzle, and F_{sp} is the self-propelled force in N. The self-propelling factor m, expressed as:

$$m = \frac{0.81A_0^2}{C^2 d_{ne}^4} S + 0.5(1+S) - \left(\frac{k}{(n_2+1)(k+1)}\right)^2 D_1^4 S + n_3 \left(\frac{1}{n_3(k+1)}\right)^2 D_3^2 \cos\theta_3 \tag{3.10}$$

where d_{ne} is the equivalent diameter of the nozzle in mm, S is the dimensionless area coefficient of the front face, D_i is the dimensionless diameter ratio of the nozzle and

orifice, *C* is the nozzle dimensionless discharge coefficient, and *k* is the dimensionless flow ratio of forward and backward orifices. The *m* factor consists of the design parameters and hydraulic characteristics of the nozzle, which are known except for the flow ratio and the discharge coefficient. The factor shows the self-propelling ability of a nozzle with a given inlet. The study indicates that for a particular nozzle, the self-propelling factor can be determined experimentally and plugged into the F_{sp} equation. The discharge coefficient and flow ratio need to be measured. A series of experiments need to be performed to obtain pressure at various flow rates and determine the discharge coefficient. Next, the flow ratio measurement system acquires groups of forward flow rates at different total flow rates, and the flow ratio can be determined.

The apparatus used by Li et al. (2015) to measure self-propelling force (**Fig. 3.9**) consists of a high-pressure plunger pump as the power source, a high-pressure hose with 9 mm ID and 14.2 mm OD and working pressure of 40 MPa with a burst pressure of 100 MPa and a 60 mm minimum bending. The nozzle configuration includes a single 0.7 mm diameter center forward orifice, five 0.7 mm diameter forward orifices angled at 15-degrees (θ_2), and six 1.0 mm backward orifice angled at 30-degrees (θ_3). The inlet diameter d_o is 9 mm. A hydraulic sensor is used with a 30 MPa measurement range and a 20 kg range load sensor is used.

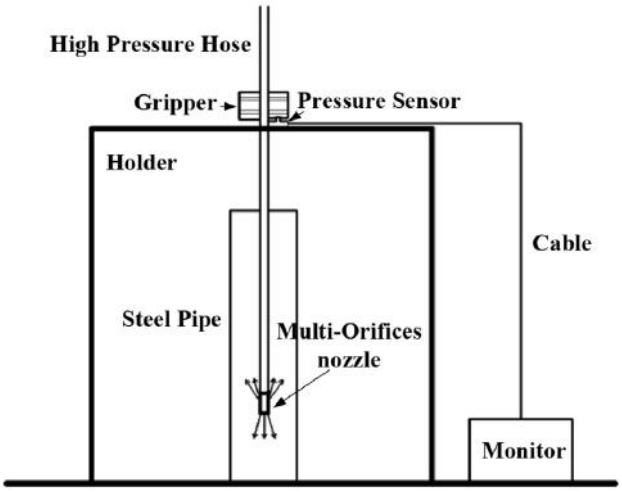

Fig. 3.9 – Schematic of test setup (Li et al. 2015)

Fig. 3.10 displays a comparative plot of calculated data versus experimental data at corresponding flow rates. The data shows a maximum difference of 4% between the calculated force and measured force, which indicates the numerical model can accurately predict the self-propelling force. The numerical model uses parameters shown in Table XX with the RNG k-epsilon turbulent model. With the back of the nozzle is selected as the inlet boundary condition and set between 6 and 25 m/s for the corresponding nozzle. Pressure outlets at the end of all orifices, set to atmospheric pressure to simulate the jet in air. The self-propelling force is obtained by first acquiring discharge coefficients, flow ratios, and total force at various flow rates. Model validation came from studying the 6+3+1 nozzle configuration, which refers to six backward orifices, three forward orifices, and a single center orifice.

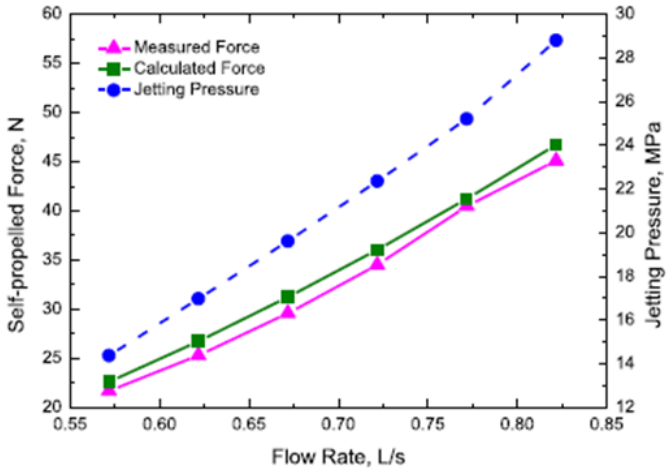

Fig. 3.10 – Measured and calculated self-propelling force versus flow rates (Li et al. 2015)

Table 3.1 numerical and calculated values of the self-propelled force (Li et al. 2015)

Number	Q_o,L/s	P_0,Mpa	F, N	Fin, N	C	k	F_{sps}, N	F_{spc}, N	Error,%
1	0.785	9.7	768.6	736.6	0.72	0.75	35.0	32.0	9.5
2	0.942	14.0	1106.6	1059.3	0.72	0.75	49.8	47.3	7.7
3	1.178	21.6	1723.7	1651.2	0.72	0.75	78.3	72.5	9.2
4	1.414	31.2	2481.6	2375.0	0.72	0.75	113.1	106.6	7.0
5	1.571	38.1	3056.4	2925.5	0.72	0.75	139.6	131.0	7.3

Li et al. (2015) looked into the effects of various design parameters, including the number of forward and backward orifices, the angle of forward and backward orifices, the diameter of orifices, and mentions the limitations. Forward orifices mainly function to crush and break the rock, but negatively affect the self-propelled ability by acting in the opposite direction. The angle of the orifices affects hole size in the front and propulsion from the backward orifices, but there exists a window of the optimum angle for forward and backward orifices. Hole diameter affects the fluid discharge properties and subsequently the self-propellability and rock-breaking capabilities.

Chapter 4 – Mathematical Modeling

An RJD hydraulic model is created by incorporating the conservation equations of mass, momentum, and energy. The model uses an empirical correlation for discharge coefficient to correct nozzle velocity, which obtained from the Bernoulli equation. The model predicts the cutting force and propulsion forces resulting from the front and backward jetting, respectively. In Addition, the tension force acting on the flexible hose can be determined. The use of the control-volume approach in the analysis helps in formulating the model based on the governing equations. In **Fig. 4.1**, the control boundary (dotted red line) denotes the control volume within and the surroundings outside.

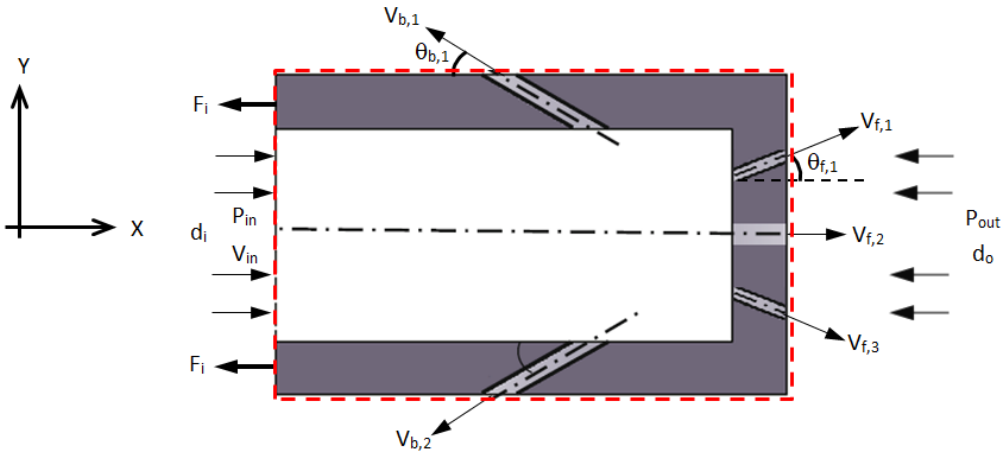

Fig. 4.1 – Forces on the jet bit (adopted from Ruichang et al. 2009)

4.1 Assumptions

The basis of a mathematical model is simplifying assumptions. This means that mathematical models provide approximate solutions, which are highly beneficial for designing and optimization. The fundamental assumptions of the new model include:

- Incompressible fluid

- Flow is under steady-state condition
- Forward and backward nozzles are treated as orifices
- The flow is isothermal
- Force due to wall shear stress is minor
- Mechanical friction force is negligible

RJD functions through three primary physical concepts or conservation principals, conservation of mass, conservation of momentum, and energy balance.

4.2 Conservation of Mass

For a control volume, the law of conservation of mass can be applied to describe the rate of accumulation of mass ($\int_{CV} \frac{\partial \rho}{\partial t}\, d\mathcal{V}$) in terms of the sum of mass flow rate entering to the control volume ($\sum(\rho_i A_i V_i)_{in}$) and the sum of mass leaving the control volume ($\sum(\rho_i A_i V_i)_{out}$). Thus:

$$\int_{CV} \frac{\partial \rho}{\partial t}\, d\mathcal{V} \;+\; \sum(\rho_i A_i V_i)_{out} \;-\; \sum(\rho_i A_i V_i)_{in} \;= 0 \tag{4.1}$$

For steady flow, the rate of accumulation of mass is zero ($\int_{CV} \frac{\partial \rho}{\partial t}\, d\mathcal{V} = 0$). Thus, mass flows in and out of the control volume balances exactly.

$$\sum_i(\rho_i A_i V_i)_{out} = \sum_i(\rho_i A_i V_i)_{in} \tag{4.2}$$

Applying Eq. (4.2) for the jet bit considered in **Fig. 4.1**, the following general expression can be obtained for incompressible fluid:

$$Q = A_{in}V_{in} = \sum_{n=1}^{N}\left(A_{f,n}V_{f,n}\right) + \sum_{m=1}^{M}\left(A_{b,m}V_{b,m}\right) \tag{4.3}$$

where A_{in} is inlet area of the jet bit. N and M are the total number of forward and backward facing nozzles, respectively. $A_{f,n}$ and $A_{b,m}$ are the areas of forward and backward facing nozzles, respectively. The mass balance equation for the jet bit shown in Fig 4.1 can be expressed as:

$$Q = A_{in}V_{in} = A_{f,1}V_{f,1} + A_{f,2}V_{f,2} + A_{f,3}V_{f,3} + A_{b,1}V_{b,1} + A_{b,2}V_{b,2} \quad (4.4)$$

4.3 Conservation of Linear Momentum

The linear momentum equation applies the Reynolds transport theorem with linear momentum as the fluid property differentiated **(White 1998)**. Applying the Reynolds transport theorem, a generalized linear momentum relation for a deformable control volume can be given as:

$$\sum \mathbf{F} = \frac{d}{dt}\left(\int_{CV} \mathbf{V}\rho \, d\mathcal{V}\right) + \int_{CS} \mathbf{V}\rho \, (\mathbf{V} \cdot \mathbf{n}) \, dA \quad (4.5)$$

V is the fluid velocity relative to an inertial coordinate system. $\sum \boldsymbol{F}$ is the vector sum of all forces acting on the control volume material considered as a free body. Equation (4.5) is a vector relation and both integrals are vectors due to the velocity term. $\mathcal{V}$ is a volume of fluid. The directions of the forces and velocities must be consistent. For one-dimensional force analysis, only one component of the force balance is considered.

$$\sum \mathbf{F}_{\boldsymbol{x}} = \frac{d}{dt}\left(\int_{CV} V_x\rho \, d\mathcal{V}\right) + \int_{CS} V_x\rho \, (\mathbf{V} \cdot \mathbf{n}) \, dA \quad (4.6)$$

The momentum-flux term ($\int_{CS} V_x\rho \, (\mathbf{V} \cdot \mathbf{n}) \, dA$) is the analogy of the mass flow rate in Eq. (4.1). Thus, under steady state flow condition, for one-dimensional uniform-velocity inlets and outlets, Eq. (4.6) further reduces to:

$$\sum \mathbf{F}_{\boldsymbol{x}} = \sum\left(\dot{m}_i V_{x,i}\right)_{out} - \sum\left(\dot{m}_i V_{x,i}\right)_{in} \quad (4.7)$$

For the jet bit considered in Fig. 4.1, a one-dimensional generalized momentum balance equation can be obtained by applying Eq. (4.7). Thus:

$$\sum \mathbf{F}_{\boldsymbol{x}} = \sum_{n=1}^{N}\left(\dot{m}_{f,n} V_{xf,n}\right) + \sum_{m=1}^{M}\left(\dot{m}_{b,m} V_{xb,m}\right) - \left(\dot{m}_{in} V_{in}\right) \quad (4.8)$$

The momentum balance for the jet bit shown in Fig. 4.1 is given in a simplified form as:

$$-F_i + P_{in}A_{in} - P_{out}A_{out} = \sum_{n=1}^{N}\left(\dot{m}_{f,n} V_{xf,n}\right) + \sum_{m=1}^{M}\left(\dot{m}_{b,m} V_{xb,m}\right) - \left(\dot{m}_{in} V_{in}\right) \quad (4.9)$$

The net momentum flux of forward facing nozzles $\left(\sum_{n=1}^{N}\left(\dot{m}_{f,n} V_{xf,n}\right)\right)$ is calculated as:

$$\sum_{n=1}^{N}\left(\dot{m}_{f,n} V_{xf,n}\right) = \dot{m}_{f,1} V_{f,1} Cos\left(\theta_{f,1}\right) + \dot{m}_{f,2} V_{f,2} Cos\left(\theta_{f,2}\right) + \dot{m}_{f,3} V_{f,3} Cos\left(\theta_{f,3}\right) \quad (4.10)$$

Similarly, the net momentum flux of backward facing nozzles $\left(\sum_{m=1}^{M}\left(\dot{m}_{b,m} V_{xb,m}\right)\right)$ is calculated as:

$$\sum_{m=1}^{M}\left(\dot{m}_{b,m} V_{xb,m}\right) = -\dot{m}_{b,1} V_{b,1} Cos\left(\theta_{b,1}\right) - \dot{m}_{b,2} V_{b,2} Cos\left(\theta_{b,2}\right) \quad (4.11)$$

Thus, the propulsion force is:

$$F_{propulsion} = \sum_{n=1}^{N}\left(\dot{m}_{f,n} V_{xf,n}\right) + \sum_{m=1}^{M}\left(\dot{m}_{b,m} V_{xb,m}\right) - \left(\dot{m}_{in} V_{in}\right) \quad (4.12)$$

4.4 Conservation of Angular Momentum

Although this study is focused on linear momentum balance, the angular momentum balance needs to be considered in the event of plugged nozzles or unbalanced

bit design. A plugged nozzle creates an imbalance in the fluid discharge and the momentum flux, changing the direction of the bit. A balance bit design ensures no moment at the connection between the bit and the hose. This means that the momentum flux generated by a given nozzle must be balanced with equal and opposite momentum flux generated by another nozzle. Hence, in order to balance the momentum fluxes, identical nozzles need to be installed in the opposite direction of the jet bit as shown in Fig. 4.1. The backward facing nozzles must be identical in size and geometry to produce equal momentum fluxes, but opposite in direction.

From Reynolds transport theorem (White 1998), a generalized angular momentum equation for stationary control volume is expressed as:

$$\sum \mathbf{M}_O = \frac{\partial}{\partial t}\left[\int_{CV}(\mathbf{r} \times \mathbf{V})\rho \, d\mathcal{V}\right] + \int_{CS}(\mathbf{r} \times \mathbf{V})\rho(\mathbf{V} \cdot \mathbf{n}) \, dA \tag{4.12}$$

$\sum \boldsymbol{F}$ is the vector sum of all moments of forces acting on the control volume material at Point O. **r** is a position vector from Point O to the nozzle exits or points where forces acting on the body are applied. For steady state flow with one-dimensional uniform-velocity inlets and outlets, Eq. (4.12) reduces to:

$$\sum \mathbf{M}_O = \sum(r_i \times \dot{m}_i V_i)_{out} - \sum\left(r_j \times \dot{m}_j V_j\right)_{in} \tag{4.13}$$

4.5 Energy Balance

For the steady isothermal flow of incompressible fluid in jetting nozzles, a generalized energy equation for a control volume with one inlet and one outlet can be written as:

$$\frac{p_{in}}{\rho g} + \frac{V_{in}^2}{2g} + z_{in} = \frac{p_{out}}{\rho g} + \frac{V_{out}^2}{2g} + z_{out} + h_v \tag{4.14}$$

Equation (4.14) can be further simplified by neglecting the inlet kinetic energy head $\left(\frac{V_{in}^2}{2g}\right)$, head lost due to viscous friction (h_v), and elevation difference across the nozzle $(z_{in} - z_{out})$. After implementing these assumptions and simplifications, the exit velocity of the fluid can be expressed as:

$$V_{out} = \sqrt{\frac{2(p_{in} - p_{out})}{\rho}} \tag{4.15}$$

Due to the eliminating of the viscous head loss, Eq. (4.15) overestimates the discharge/exit velocity of the fluid. Therefore, the discharge coefficient $(C_{d,i})$ is often used to account for the friction losses, where the subscript 'i' refers to which particular orifice. Thus, fluid velocity at the nozzle exit is accurately determined by:

$$V_{out,i} = C_{d,i}\sqrt{\frac{2(p_{in} - p_{out})}{\rho}} \tag{4.16}$$

The coefficient of nozzles/orifices are functions of the discharge Reynolds number $\left(Re_{D,i} = \frac{\rho V_i d_n}{\mu}\right)$, diameter ratio ($\beta$ = d_n/d_i) and aspect ratio ($L_i/d_{n,i}$), where L_i and $d_{n,i}$ represent the thickness and the diameter of the orifice. For orifice with low diameter ratio, the discharge coefficient is a function of Reynolds number and aspect ratio. According to Bohra (2004), the discharge coefficient is determined using the following equations:

$$0.0 < \frac{L}{d} \leq .9: \quad C_d = 0.255\left[1 + \left(\frac{L}{d}\right)^{2.195}\right] + \frac{0.356}{\left(1+\left(\frac{L}{d}\right)\right)^{0.140}} \tag{4.17}$$

$$0.9 < \frac{L}{d} \leq 2.5: \quad C_d = 0.876 - 0.0139\left(\frac{L}{d}\right) - \frac{0.084}{\left(\frac{L}{d}\right)} \tag{4.18}$$

$$2.5 < \frac{L}{d} \leq 9.5: \quad C_d = 0.292\left[1 + \left(\frac{L}{d}\right)^{-0.068}\right] + \frac{0.292}{\left(1+\left(\frac{L}{d}\right)\right)^{0.150}} \tag{4.19}$$

These equations come from the improved correlation of data provided in Ward-Smith (1971) by Morris and Garimella (1998). This correlation offers an improvement of the Ward-Smith equations, but according to Morris and Garimella are valid for $\beta \leq 0.0635$. Whereas, Bohra states this correlation works for $\beta < 0.25$, but only tested with a maximum $\beta = 0.137$.

4.6 Discharge Coefficient

Using a similar approach as Morris and Garimella, combining data from Ward-Smith and Lichtarowicz et al. (1965) allows for slight improvement on equations 4.17-4.19 above with more data points. The plot in **Fig. 4.2** displays aspect ratio versus discharge coefficient data gathered from Lichtarowicz et al. (1965) and Ward-Smith (1971) labeled with their corresponding authors. The red arrows labeled 1, 2, and 3 follow the contour of the plot, showing the change in slope and the cutoffs for Eq. 4.17-4.19. The plots shows a sharp increase in discharge coefficient from an aspect ratio of zero until slightly under one, the slope becomes more gradual until it reaches the peak C_d at an aspect ratio around two or slightly over two, then gradually declines as the aspect ratio increases. By separating Fig. 4.2 into three plots, an optimum trend equation obtained for each and compared with the equations from Morris and Garimella (1998). Seeking to simplify the correlation from three equations to a single equation, plugging the data into the 'DataFit' software and running all non-linear regression models resulted in

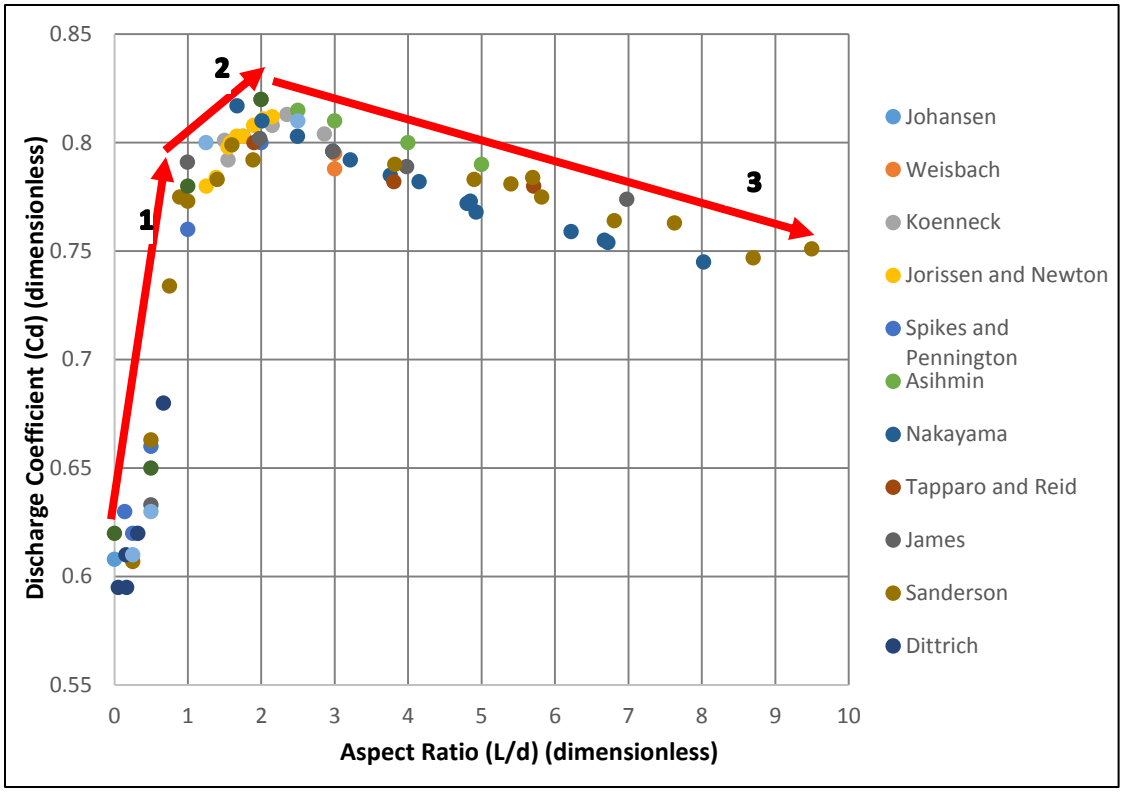

Fig. 4.2 – Plot of aspect ratio vs discharge coefficient through orifices (data acquired from Lichtarowicz et al. (1965) and Ward-Smith (1971))

polynomial equations being the six best line fits and equation seven being an exponential equation. The fifth-degree polynomial (Eq. 4.20) and exponential equation (Eq. 4.21) appear to plot the best with the data, understanding the sensitivity of polynomial equations with limited data points. Both of these equations plotted in Fig. 4.3 with the discharge coefficient data points. Equation (4.20) produces a coefficient of multiple determination (R^2) of .9357, while equation (4.21) obtains an R^2 value of .9292, both covering a range of aspect ratios from 0-9.5.

$$C_{d,i} = 0.000067536\left(\frac{L_i}{d_i}\right)^5 - 0.00200928\left(\frac{L_i}{d_i}\right)^4 + 0.0227695\left(\frac{L_i}{d_i}\right)^3 - 0.121037\left(\frac{L_i}{d_i}\right)^2 + 0.2867\left(\frac{L_i}{d_i}\right) + .56623 \quad (4.20)$$

$$C_{d,i} = 0.97346 - 0.082363\left(\frac{L_i}{d_i}\right)^{1/2} - 0.38869e^{\left(-\frac{L_i}{d_i}\right)} \quad (4.21)$$

Although, looking at the data, the discharge coefficient seems to level out at an aspect ratio around 7-8. Most orifices will not exceed an aspect ratio of seven or eight, but it is entirely possible. The key drawbacks from these equations are the inaccuracy outside of the sample range of aspect ratio. Equation (4.21) maintains an adequate calculation up to an aspect ratio of roughly 7, but from the data and noticing a flattening of the discharge coefficient, the value assumes constant beyond that point. The same goes for Equation (4.20) up to an aspect ratio of 8.5, anything beyond assumes a constant value.

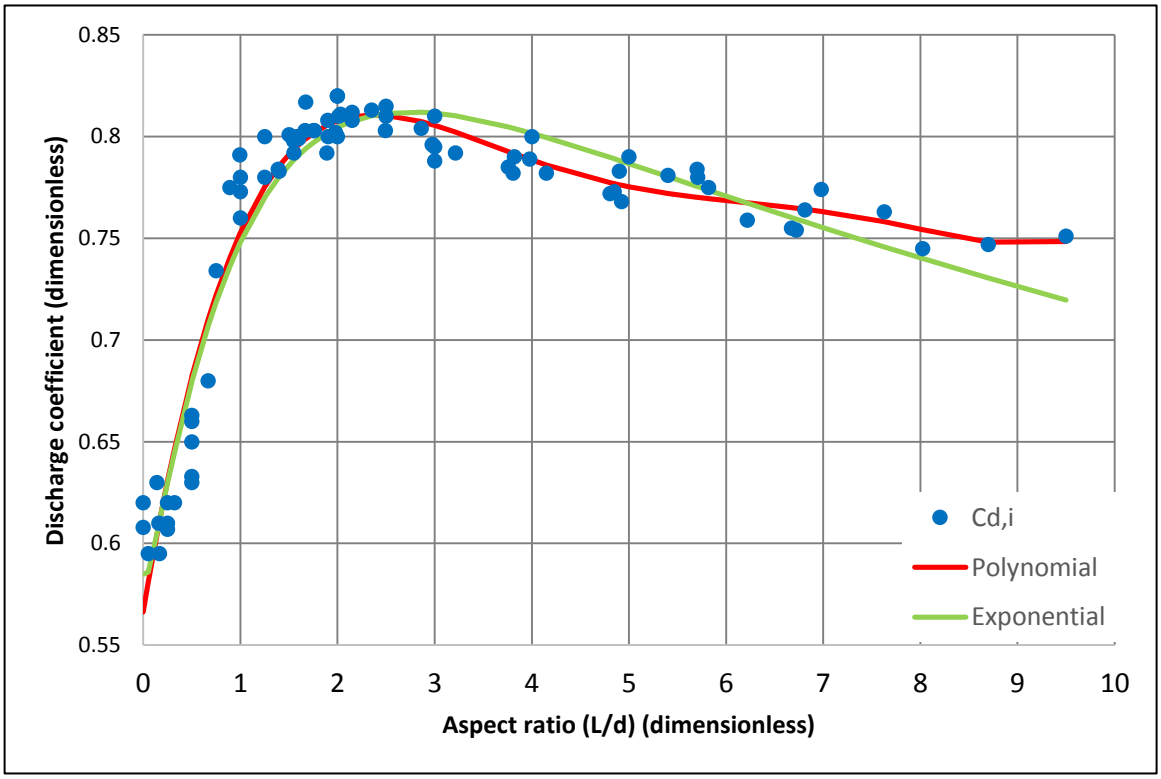

Fig. 4.3 – Plotted data from Ward-Smith (1971) and Lichtarowicz (1965) with aspect ratios from 0-9.5 alongside Eq. 4.20-4.21.

Chapter 5 – Experimentation

5.1 Test Scope

The scope of this experiment investigates the resultant discharge coefficient over a range of flow rates for four different diameter orifices. Using a predetermined orifice diameter with a range of flow rates obtains data points for discharge coefficients with the assumption that the data will coincide with the data from Ward-Smith (1971) and Lichtarowicz (1965). Using a range of flow rates leads to a range in Reynolds numbers and changing the diameter of the orifice subsequently changes the aspect ratio. By monitoring these variables allows for better comparison to previous data and literature. An accurate estimate of discharge coefficient leads to a greater accuracy of the RJD force model.

5.2 Test Set-up

The concept behind experimental set-up uses the pump to generate pressure resulting in a higher fluid flow out of a small diameter orifice. That fluid creates an equal and opposite force termed the discharge force when exiting the bit, which is noticed through the force sensor attached to the steel frame above. Shown in the test loop schematic depicted in Fig. 5.1, the testing set-up includes the following components: i) Water source; ii) Dayton Electric pump model 3Z660E has a 2.2 gpm capacity, a pressure rating of 700 psi, and a power output of 1 HP; iii) Omega flow sensor model FLR1013ST-I with an operating range of 1.0-10.0 L/min; iv) Ashcroft 3,000 psi pressure gauge; v) MEAS pressure sensor model PRESS XDCR M3041-000005-2K5PG with a pressure rating of 2,500 psi; vi) Temperature gauge; vii) T-fitting rated to 3,000 psi; viii) Cross fitting rated to 3,000 psi; ix) High-pressure ball valve rated to 3,000 psi; x) High-pressure

hose (x2) rated to 2,000 psi; xi) Flexible hose; xii) Drain hose made from a regular garden hose; xiii) Front nozzle bits (x8) with four brass bits, four steel bits and one brass back nozzle bit; xiv) Clear tubing to help contain the fluid; xv) Fluid collection container; xvi). MARK-10 digital force gauge had a capacity of 5 lbf, 2.5 kg, and 25 N, gave an output display in Newton to two decimal places (accuracy of ± 0.02 N).

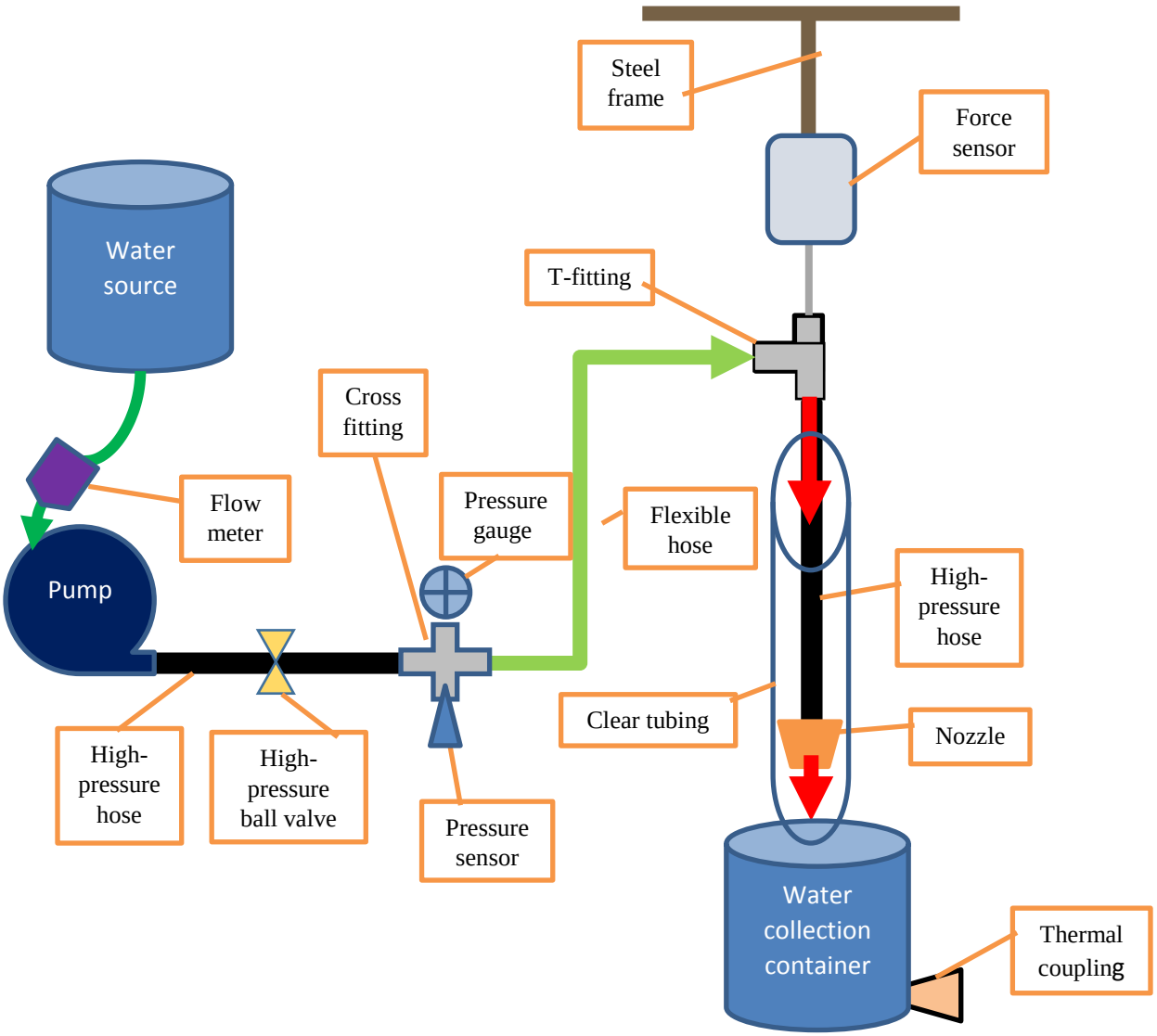

Fig. 5.1 – Test loop schematic.

The RJD experiments conducted used the Omega flow sensor, Dayton Electric pump, MEAS pressure sensor, and MARK-10 digital force gauge. Both the pressure

sensor and flow meter were wired to separate mutlimeters as an output display. The GE2524 Digital Multimeter connected to the pressure sensor gave a display of 1-4 volts (V) for a pressure range of 0-2500 psi. The Southwire 10030S Manual Ranging Multimeter connected to the flow meter gave a display of 4-20 milliamps (mA) for flow rates from 0-10 liters per minute (L/min).

5.3 Test Procedure

The nozzles tested, listed in Table 5.1, include four 4140 steel nozzles at four different diameters and four brass nozzles at four different diameters. A brass bit drilled with two 45-degree angle backwards facing nozzles paired with each brass nozzle to create four configurations containing nozzles in opposite directions. Any data omitted from this section can be found in the appendix.

Preparing the nozzles required a hole to be drilled into the front pipe fitting. Understanding that the size of the hole will not be the same size as the bit, the nozzle diameters needed to be accurately measured. To do this, a microscopic picture was taken of each nozzle with a stencil with a known diameter overlaid as a point of reference, like the one shown in **Fig. 5.2**. Using AutoCAD to measure both diameters to get the ratio and multiply by the known stencil diameter provides the measurement of the nozzle diameter.

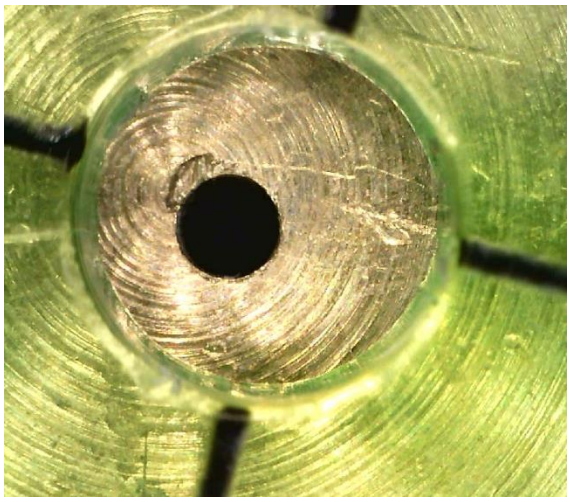

Fig. 5.2 – Microscopic photo of a brass nozzle with a reference stencil overlaid.

Table 5.1 – Nozzle Dimensions

Nozzle	Material	Nozzle diameter	Nozzle length	Aspect ratio
		(mm)	(mm)	(Length/diameter)
1	Brass	0.89318	2.3	2.5750
2	Brass	1.07289	2.25	2.0971
3	Brass	1.4058	2.31	1.6432
4	Brass	1.5846	2.29	1.4451
5	Steel	1.0835	6.842	6.3144
6	Steel	1.4334	6.95	4.8487
7	Steel	1.7064	7.646	4.4808
8	Steel	1.8383	7.2	3.9166

Table 5.2 – Nozzle Combinations

Array	Nozzle type	Nozzle diameter (mm)	Nozzle length (mm)	Aspect ratio (Length/diameter)
1	Front	0.89318	2.3	2.5750
	Back	1.6	6	3.75
2	Front	1.07289	2.25	2.0971
	Back	1.6	6	3.75
3	Front	1.4058	2.31	1.6432
	Back	1.6	6	3.75
4	Front	1.5846	2.29	1.4451
	Back	1.6	6	3.75

Table 5. 2

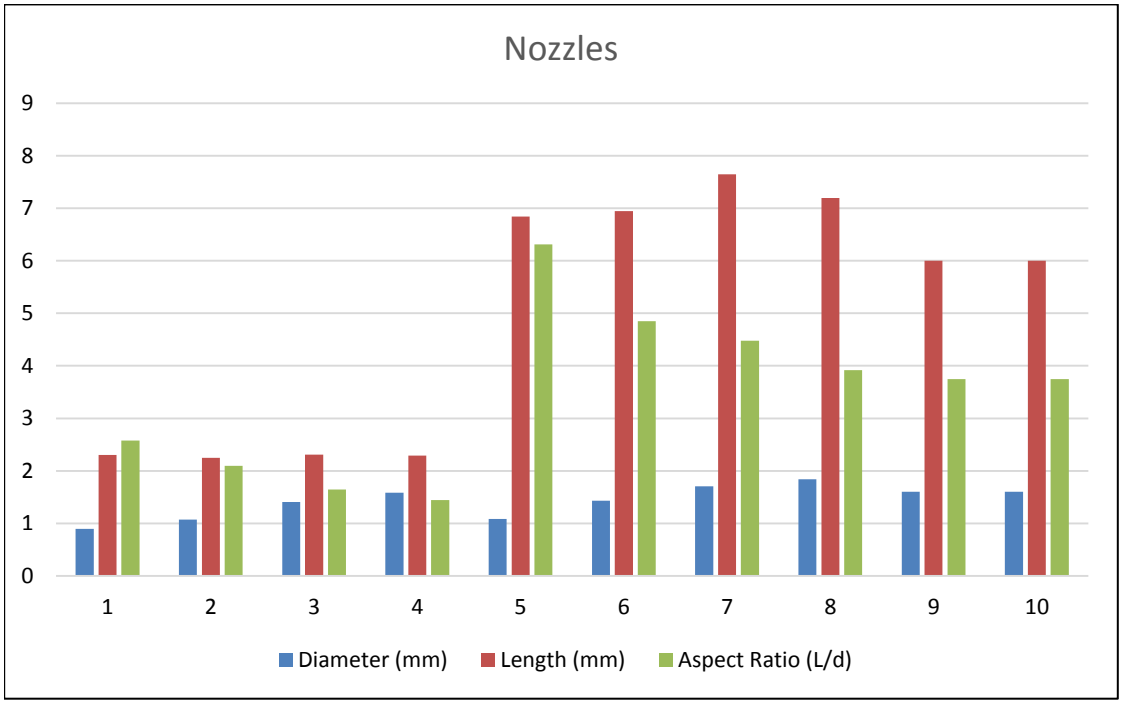

Fig. 5.3 - Chart of nozzle dimensions with 1-8 being front nozzles and 9-10 being back nozzles.

Step 1. Preparation: All electronics are plugged in and all readings are check to ensure proper function.

Step 2. Calibration: Water is turned on and again all data displays are checked to ensure everything is functioning correctly. Any air trapped in the system is removed. The flow rate is throttled down using a high-pressure ball valve and the force sensor was tared before each trial to account for the weight of the water, hose, and nozzle.

Step 3. Testing: The valve is opened completely and the pump is turned on. Once flow rate, pressure, and force level out this data is recorded. With the ball valve, flow rate is incrementally throttled down and data recorded at each instance.

5.4 Test Results

This section goes through the data obtained from the experiments. Each test used strictly domestic water from the City of Norman with a temperature of 68F (± 0.5 deg. F). The flow data for each nozzle is presented on a scatter plot of pressure in psi on the x-axis and flow rate in gallons per minute (gpm) on the y-axis. The force data for each nozzle is presented on a scatter plot of pressure in psi on the x-axis and force in Newton on the y-axis. The six plots presented in this section provide data for a single forward brass nozzle, a single forward steel nozzle, and a combination of forward and backward nozzles. The model plotted used the pressures obtained during testing applied with the discharge coefficient correlation discussed in Section 4.6. For the combination nozzles, two discharge coefficients were applied separately to the front and back nozzles to

calculate differing exit velocities from Equation 4.16. For each of the single front nozzles a theoretical range of Reynolds number was calculated (discussed in section 4.5), meaning the discharge coefficient was not applied.

Fig. 5.4 gives plots of flow rate vs pressure and back force vs pressure for a single front brass orifice with a diameter of 1.585 mm (Nozzle 4). **Fig. 5.5** gives plots flow rate vs pressure and back force vs pressure for a single front steel orifice with a diameter of 1.084 mm (Nozzle 5). **Fig. 5.6** gives plots flow rate vs pressure and propulsion force vs pressure for a brass nozzle configuration of one front nozzle with a diameter of 1.406 mm and two back nozzles with diameters of 1.600 mm (Nozzle combination 3).

From the flow rate plots (Fig. 5.4a, 5.5a, 5.6a), the experimental data tends to deviate from the model prediction the larger the flow rates become. A couple reasons for this may be the flow meter is not accurate enough for the flow rates required or losses across the flow meter occur due to the constriction in the flow path from 1.5 in to 0.25 in and back to 1.5 in coupled with slight frictional losses in the system. For the single nozzle tests, the data flow rates compared to the model appear similar, but deviated the larger the flow rate became. This could help understand why the flow rates were so different for the combination nozzles; the larger flow area forces a larger initial flow rate. The difference between data and model only increases with an increased flow rate. The model and data do not line up exactly with the model often being slightly high, this could be for a couple reasons. The first being frictional losses in the system, with hoses being small diameter, this leads to a greater frictional effect. Another reason could be the constrictions within the system, for fluid to flow across the flow meter; the fluid goes from 1.5 in hose to 0.25 in flow meter and back to 1.5 in and into the suction side of the

pump. This may be the cause of error in the flow reading or something may be malfunctioning with the flow meter itself. Although, flow rate is not imperative for the model to function, this is a parameter in the field highly focused on and often used as a check for most operations.

From the force plots (Fig. 5.4b, 5.5b, 5.6b), the experimental data and model prediction correlate well with a maximum difference of 1.5 N and average difference of 0.37 N. As a percentage the maximum difference is 491%, this happens when the experiment data obtains a 0.12 N reading while the model predicts 0.71 N. Although, only a difference of 0.59 N, it is important to mention both in this case because a 491% difference suggests the models is inaccurate, but the 0.59 N difference puts this into perspective. The average difference of 14% reduces to 7% when three outlier points of 491%, 225%, and 179% are removed. By omitting the three data point over 100% difference, cuts the percent error of the model in half. Again, omitting the next five outliers, all 44% or greater, the average difference reduces further to 5%, this indicates an accurate model adequate for predicting RJD forces. This also implies the discharge coefficient correlation from Section 4.6 provides an adequate prediction from simply the length and diameter of an orifice.

Validating the model through experimentation allows for future improvement when designing and optimizing jetting bits. The model also helps with looking at operating pressures, will the working material have the ability to handle these pressure loads. This model can also lay the groundwork to study the ROP for several optimized bits. Although, the forces seem to agree between data and model, a better flow measurement or better accuracy would on further confirm the validity of the model.

Nozzle 4

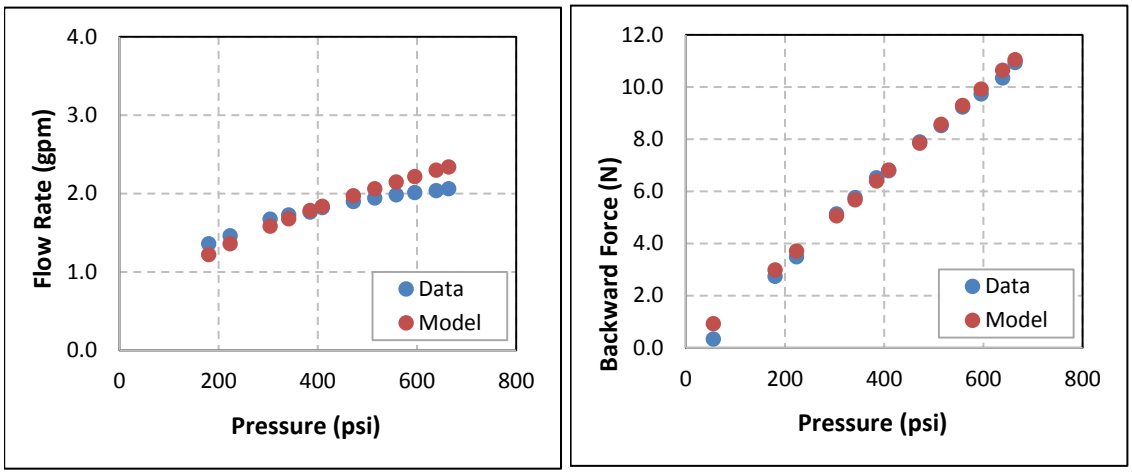

(a) **(b)**

Fig. 5.4 – Results for single orifice with a diameter of 1.585 mm and aspect ratio of 1.45: a) flow rate vs pressure; and b) backward force vs. pressure

Nozzle 6

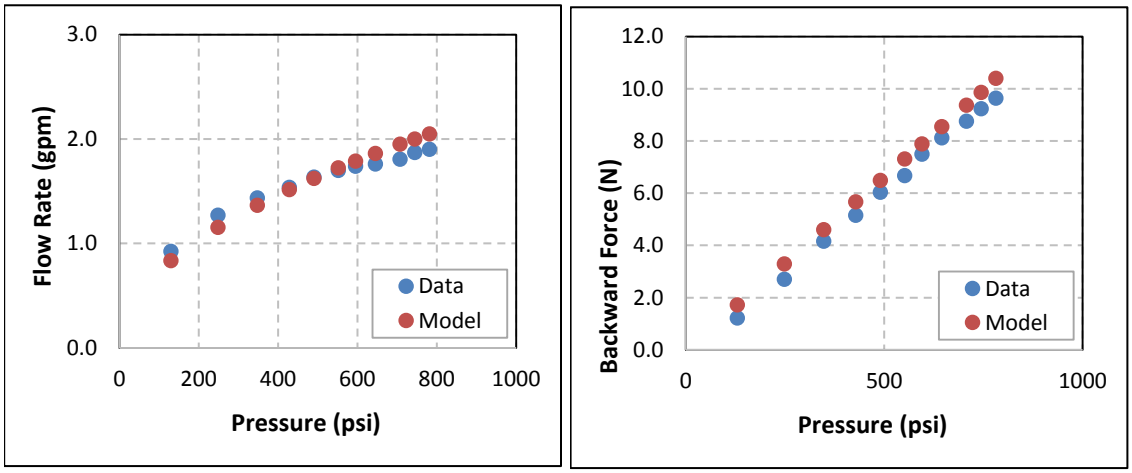

(a) **(b)**

Fig. 5.5 – Results for a single front orifice with a diameter of 1.433 mm and aspect ratio of 4.85: a) flow rate vs. pressure; and b) backward force vs. pressure

Nozzle Combination 3

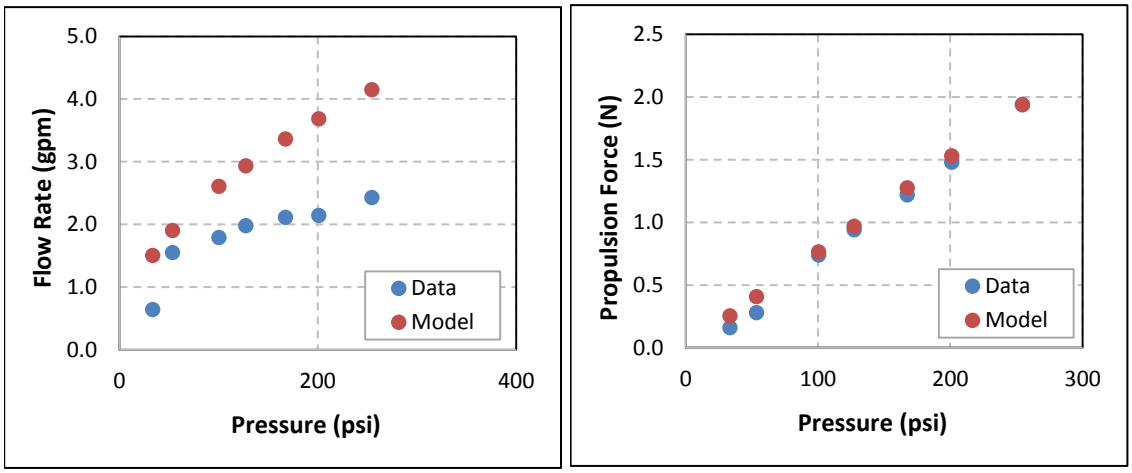

(a) **(b)**

Fig. 5.6 – Results for a nozzle with one front orifice with a diameter of 1.406 mm and aspect ratio of 1.64, and two back nozzles angled at 45-degree toward the back with diameters of 1.6 mm and aspect ratios of 3.75: a) flow rate vs. pressure; and b) propulsion force vs. pressure

Chapter 6 – Model Comparison and Parametric Study

6.1 Model Comparison

The purpose of this section sought to analyze and compare the measured data from Li et al. (2015) when plugged into the newly developed model. Li et al. (2015) operated at significantly higher pressure than the tests conducted in this thesis study, but theoretically, the model should retain the accuracy when predicting other measurements. The thinking is perhaps some of the same questions or concerns were encountered regarding flow measurements or data acquisition.

Li et al. (2015) focused on a 6+3+1 bit design, which means six back nozzles, three front nozzles, and one front center nozzle. Various configurations to the 6+3+1 bit design mentioned in the paper, but not specified in the table of data provided. The nozzle

configuration that gave the best comparison was six back nozzles with diameters of 1.2 mm, angled at 45-degrees; three front nozzles with diameters of 1.2 mm and no angle; and one front center nozzle with a 1.2 mm diameter. This is the nozzle configuration used for the model predictions in **Fig. 6.1**. The discharge coefficients range from 0.5 – 1.0 for the flow rate plot and from 0.6 – 1.0 for the propulsion force plot.

In Fig. 6.1, the red data points represent the measured data from Li et al. (2015), while the lines represent model predictions for various discharge coefficients. Fig. 6.1a shows a consistent trend between model predictions and the measured data, and a near identical trend when the discharge coefficient is set to 0.5. From the discharge coefficient correlation developed in Section 4.6, the aspect ratio must be almost zero for this to occur. Understanding that jet drilling consists of high pressures, the material must be thick enough to withstand operating pressures, which means a larger aspect ratio. This means that the model predicts a higher flow rate than measured. This is the same issue encountered when testing the back jetting nozzles in this study.

Fig. 6.1b displays a consistent trend with the propulsion force prediction and measured data. The difference here is the model prediction aligns well with the data at a discharge coefficient of 0.78, which is consistent with the ones used in the Section 5.4 and the correlation developed. Again, this seems to be the same issue where the propulsion force prediction remains accurate, while the flow rate prediction remains high consistently.

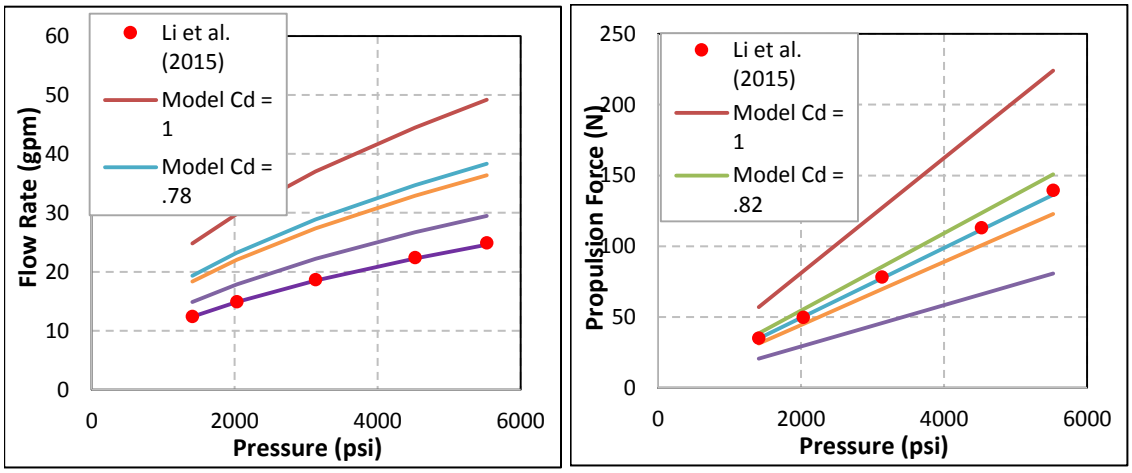

(a) **(b)**

Fig. 6.1 – Results using pressure data from Li et al. (2015) and a 6+3+1 nozzle configuration for various discharge coefficients; nozzle diameters set 1.2 mm diameter; front nozzles angle set to 0-degrees and back nozzles angle set at 30-degrees: a) flow rate vs pressure; and b) propulsion force vs. pressure

With the same concern noticed using data from elsewhere, this only poses more questions moving forward. Perhaps it is the geometry of the nozzle and the path of the flow, which is having to aggressively change direction at a 135 – 150-degree angle. Perhaps there are more losses in the system than anticipated, but this should effect the propulsion force also. The propulsion force comes from momentum flux terms and the momentum comes from the fluid flow, thus should change the propulsion forces. This does not appear to be the case and should be investigated further.

6.2 Parametric Study

The purpose of the parametric study looks at the influence of each parameter on force and flow rate. From this comes a better understanding on which parameters have more significance when looking to optimize a bit configuration. This study focuses on the effects of nozzle diameter, angle, and number of nozzles for both front and back nozzles. The study is broken into front and back nozzles. From the front nozzles, the study looks at the influence of nozzle diameter. From the back nozzles, the study looks at the influences of nozzle diameter, number of nozzles, and nozzle angle. The study remains theoretical by holding constant the discharge coefficient at one and pressures (50 -1000 psi) the same for each nozzle.

The first parameter in this study is the effect of nozzle diameter from a single nozzle on flow rate and force. Using nozzle diameters ranging from 0.8 - 1.8 mm, **Fig. 6.2a**, displays the output flow rates for the same pressures for six different nozzle sizes. This indicates that flow rate increases with an increase in nozzle at the same pressures. The plot in **Fig. 6.2b** provides a log-log plot of flow rate versus force over the same

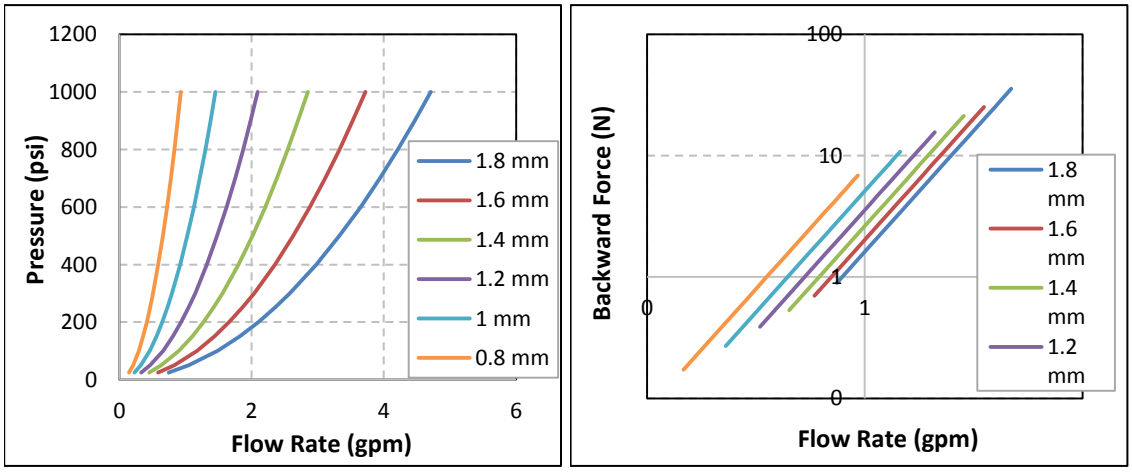

(a) **(b)**

Fig. 6.2 – Results for six different single front nozzle diameters: a) flow rate vs. pressure; and b) backward force vs. pressure

pressure range. Fig. 6.2b the resultant force increases with diameter also at the same working pressures. Both of these trends make sense theoretically, while holding pressure constant, a larger flow area leads to a larger flow rate, which leads to a larger discharge force.

The first parameter looked at for the back nozzles is the effects of the number of nozzles, the number ranging from two to eight at a 1.0 mm diameter and 45-degree angle for each nozzle. **Fig. 6.3a** shows an obvious trend of an increased flow rate with a greater number of nozzles. Again, this makes sense because more nozzles mean more area for fluid to flow. **Fig. 6.3b** shows a definite trend of force increasing with the number of nozzles, but one thing to notice is the increase in force between two nozzles and three nozzles is significantly greater increase from seven nozzles to eight nozzles. This indicates there is an optimum number of nozzles and by simply adding more nozzles may not lead to the increased force as expected. This is a key parameter when it comes to designing a jetting bit to exert enough propulsion force to penetrate into the formation,

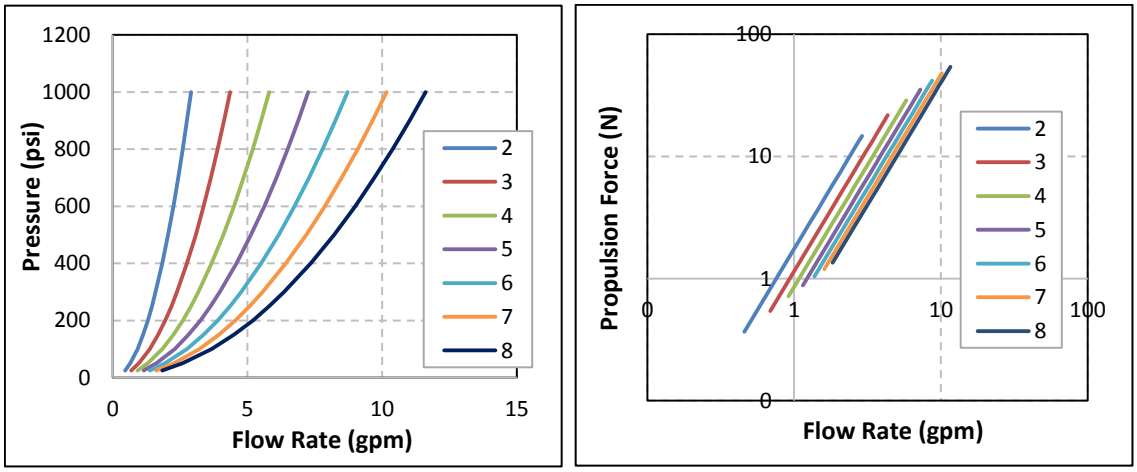

(a)a) **(b)**

Fig. 6.3 – Results for different numbers of back nozzles only using the same 1 mm diameter for each orifice: a) flow rate vs. pressure; and b) propulsion force vs. pressure

but not to overtake the ROP from the front nozzles.

The next parameter for the back nozzles, hole size, plays a factor into the design of the jetting bit. Similar to Fig. 6.2, **Fig. 6.4a** displays an increased flow rate with an increased nozzle diameter. Unlike the previous force plot for the number of nozzles, **Fig. 6.4b** shows a consistent increase in force from one nozzle diameter to the next. Although, the force increase due to increased diameter is more predictable from one size to the next, figuring out the number of back nozzles seems to be more important to avoid unnecessary losses.

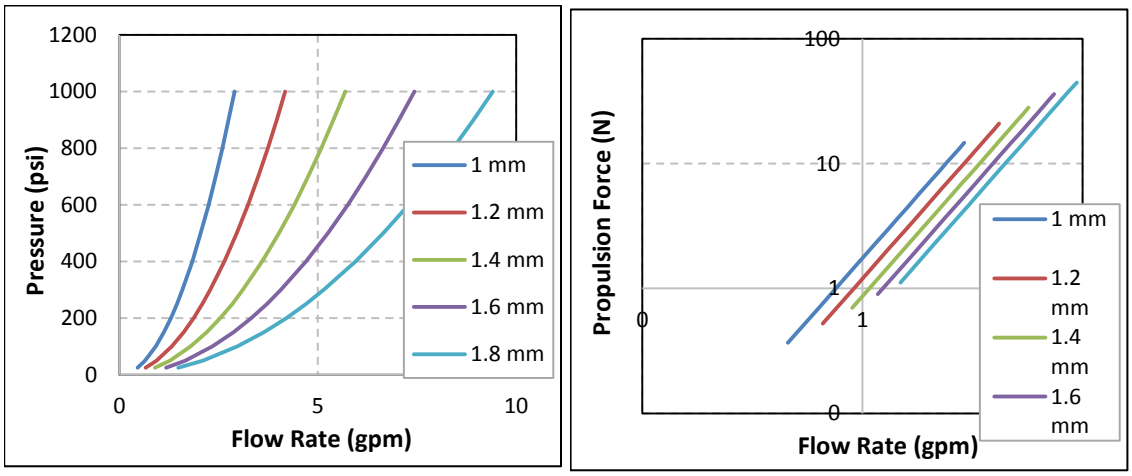

(a) **(b)**

Fig. 6.4 – Results for different diameters of back nozzles using two each of the same size and angle of 45-degrees: a) flow rate vs pressure; and b) propulsion force vs. pressure

The final parameter is the nozzle angle. From a theoretical standpoint, changing the nozzle angle does not change the discharge area, which should lead to little or no change in flow rate. These plots used to back nozzles at 1.0 mm diameter. This theory portrayed in **Fig. 6.5a** with the flow rate data from four different angles lying on top of each other. Although, no changes were intended, this is different when it comes to the force. **Fig. 6.5b** provides the difference in force of four different angles. As the angle decreases to zero, the force increases, which makes sense with a zero-degree angle being equal and opposite of the center front nozzle. Data from Fig. 6.5b appears to bunch up near one another even with a 30-degree change. This indicates that the nozzle angle

slightly effects propulsion force, but number of nozzles and the diameter become more important.

This parametric study looked at three parameters nozzle diameter, number of nozzles, and nozzle angle, and how they influence force and flow rate within the RJD system. From this parametric study, the parameters tested can be assigned a degree of importance when designing a jetting bit. For the front nozzle, the diameter will affect the

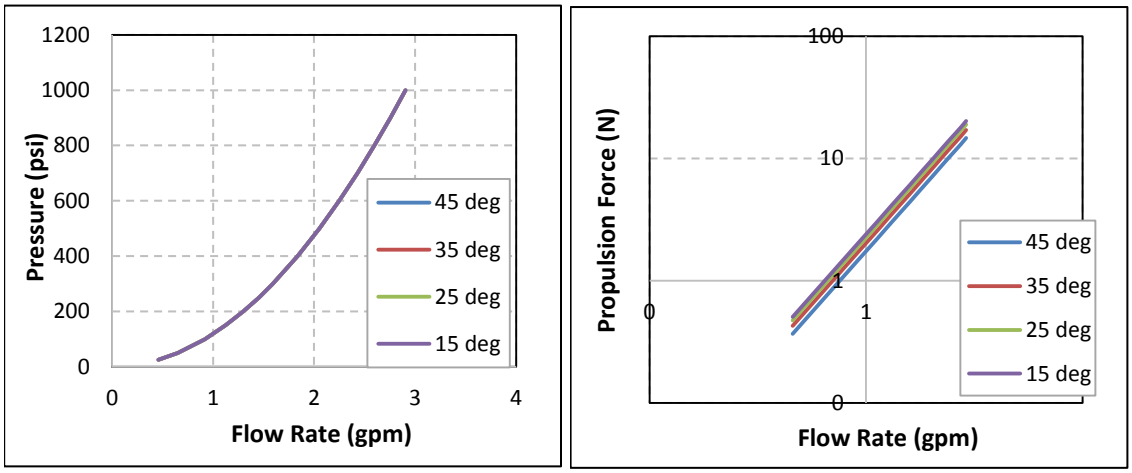

(a) **(b)**

Fig. 6.5 – Results for various angles of back nozzles using two back nozzles with the same 1 mm diameter: a) flow rate vs pressure; and b) propulsion force vs. pressure

flow rate and propulsion force, so it is key the diameter not be too large that the back nozzles cannot propel the bit into the formation. For the back nozzles, determining the optimal number is priority, to few and the bit cannot penetrate the formation and too many leads to unnecessary losses. The diameter is also important and has a significant effect on the resultant forces and flow rates. The diameter for the back nozzles must be large enough to overcome the force of the front nozzle to advance into the rock. Lastly, the nozzle angle essentially has little effect on flow rate and a minor impact on the discharge force. From this model, hundreds of nozzles configurations can be tested and compared to determine the most optimal combination of nozzles and the geometry.

Chapter 7 - Conclusions

From the thorough literature review of relevant information regarding RJD, this study touches on the system and its development, field and production studies, and modeling or other theoretical studies. The system development goes through the humble beginnings and show that adopting certain concepts allowed the RJD system to be more applicable. Leading to a vastly improved technology there is still much apprehension to deploy the technology.

The field studies look at where RJD has been applied and try to gauge the success in terms of time, cost, and production. These studies come from all over the world including the United States, Argentina, Canada, and China. Many of the studies show an improvement in production, but some also ran into operational issues, which is typical when using an unfamiliar system or technology.

Theoretical studies looked into proving conceptual ideas or theories such as the ultrashort radius concept, which has proven to be a success for the RJD system. This also led to modeling of the forces and pressure drop across a jetting bit. Although, these studies were great and set the framework for many studies after, replicating the results was difficult. This left room for improvement for a new model to focus on.

Modeling is used to predict the forces of a jetting bit at operational pressures. The model assume constant temperature of the fluid, incompressible fluid, steady flow, orifices act as nozzles, and no wall shear. This helps to simplify the model and approach this issue with a more macroscopic approach. Based on mass conservation, momentum balance, and energy balance this model is easier to understand and replicate. The model

incorporates the various parameters that go into the jetting process, which allows finding the optimum nozzle configuration.

In an effort to validate the model, test ran on numerous nozzles track flow and force data. Eight nozzles tested steel and brass, various lengths, and various hole sizes ranging from 0.8 mm to 1.8 mm. These tests ran over a range of flow rates of 0.25gpm to 2.7gpm while recording pressure and force. Results presented in plots of pressure vs flow rate and pressure vs force. The data compares to the model to data obtained during testing to analyze the prediction to tangible data points.

Utilizing already published data, the model comparison looked to compare the accuracy of the newly developed model. Although, previous literature tested at significantly higher pressures the model maintained the adequacy predicting the resultant force, but overestimated the flow rate, similar to the experiments with back jetting nozzles. The data appears to sustain the momentum from the fluid, while simultaneously losing flow rate.

A parametric study focused on a few nozzle parameters to determine the influence on the jetting bit. Front nozzles looked into the different hole sizes from 0.8mm to 1.8mm for both steel and brass bits. Back nozzles looked into the different hole size, number of nozzles, and nozzle angle. Understanding how much of an influence these parameters have and how they affect the bit design is crucial for optimization.

Analyzing the experimental data and comparing with the model, the following conclusions are drawn:

- Understand the forces present with a high-pressure multi-orifice jet bit.

- This study developed a generalized mathematical force model to predict discharge forces and flow rates.
- The discharge coefficient correlation is adequate to predict losses across an orifice, but simplifies many parameters into an easily measured diameter and aspect ratio. The correlation polynomial correlation holds only when the aspect ratio of the nozzle remain between 0 and 9.5, greater than 9.5 the correlation becomes unpredictable. The exponential correlation may be used for aspect ratios greater than 9.5.
- Experimental investigation validated the generalized model having an average difference of 5% between measured data and model force prediction and an average difference of 8% between measured data and flow rate prediction for a single front orifice. Experimental data and model predictions for flow rate deviated when incorporating backward nozzles with data differing from 24 – 40%.
- Determine the degree of influence from a few different parameters with number of nozzles, nozzle diameter, and nozzle angle from most important to least important.
- The flow rate reduction phenomena while maintaining the predicted force appears when the model is applied to already published data and should be investigated further.

7.1 Recommendations and Error Propagation

RJD must remain in sight as a stimulation method for years to come with its ease and economic viability. There is a particular niche in the market for someone willing to take the risk of deploying RJD systems to stimulate or stimulate existing wells. Continuing the study of RJD and the system can improve the technology and its viability in the future.

Although, progress made with this study, errors in the system and set up appeared throughout the testing process. Starting from the water source, the 1.5-inch diameter hose ran into the 0.25-inch diameter flow meter, a constriction like this affects the fluid flow. Along with the constriction, the numerous fittings needed to make the set up work caused a significant amount of friction to the point the flow meter could not render any reading. To help mitigate the friction, the fittings were swapped out for 0.25 to 1.5-inch swedges on both sides of the flow meter. Another issue with the flow meter was the placement, common practice place the flow meter flat with 2 – 3 ft straight piping on both sides of the meter to maintain accuracy, but only had 1 ft downstream of the flow meter in this case. From the flow meter, fluid ran into the suction side of the pump, another possible error. This did not allow the flow to become steady before entering the suction side of the pump. With the pump, errors stem from the piston strokes, it is impossible to have identical stroke lengths for every stroke so minor oscillations often noticed in the flow readings. Downstream of the pump the fluid ran through a ball valve used to control the flow rate, creating another constriction. This flowed into the flexible hose and attached to the T-fitting, which was an abrupt change in direction in the flow path. From here, the flow went through the last of the high-pressure hose and out the nozzle bit.

Moving forward, this study looks to improve on:

- Flow measurement, the flow meter used did not seem to provide correct values or could not handle the rates needed for testing. Along with this, limiting the number of constrictions in the flow system would also benefit the flow measurement.
- Consider moving the point where flow rate is measured as close to the bit as possible to investigate the flow reduction phenomena.
- Nozzle bits, including the size of the hole drilled and the shape (whether the hole is straight). Any imperfections within the nozzle will have a direct effect on the resultant forces and measurements, so it is best to have the nozzle hole drilled as clean and straight as possible.
- Look into other parameters to study and test, such as rate of penetration to extend the research beyond this study.
- Generate a second model with flow rate as the input to use as a comparison on how well flow rate, pressure, and force align with each other.

References

Bin, W., Gensheng, L., and Zhongwei, H. 2016. Hydraulics Calculations and Field Application of Radial Jet Drilling. *SPE Drilling & Completion* 31 (1): 71—81. SPE-179729-PA. http://dx.doi.org/10.2118/179729-PA.

Bohra, L.K. 2004. Non-Dimensional Analysis and Model Development. In Flow and Pressure Drop of Highly Viscous Fluids in Small Aperture Orifices (Orifice Model Developement) Chapt. 5. Georgia Institute of Technology.

Bruni, M.A., Biasotti, J.H., and Solomone, G.D. 2007. Radial Drilling in Argentina. Presented at the Latin American & Caribbean Petroleum Engineering Conference, Buenos Aires, Argentina, 15—18 April. SPE-107382. http://dx.doi.org/10.2118/107382.

Buckman, W.G., Buckman, Z.P., and Maurer, W.C. 2013. A new approach to drilling. Hydrocarbon Engineering, *Oilfield Technology* 2 (8): 37—40.

Buset, P., Riiber, M., and Eek, A. 2001. Jet Drilling Tool: Cost-Effective Lateral Drilling Technology for Enhanced Oil Recovery. Presented at the Intervention and Coiled Tubing Association - Coiled Tubing Roundtable, Houston, Texas, 7—8 March. SPE-68504. http://dx.doi.org/10.2118/68504.

Chi, H., Li, G., and Huang, Z. 2015. Maximum Drillable Length of the Radial Horizontal Micro-Hole Drilled with Multiple High-pressure Water Jets. *Journal of Natural Gas Science and Engineering* 26: 1042—1049.

Chi, H., Li, G., and Liao, H. 2016. Effects of parameters of self-propelled multi-orifice nozzle on drilling capability of water jet drilling technology. 86, *International Journal of Rock Mechanics and Mining Sciences*: 23—28. http://dx.doi.org/10.1016/j.ijrmms.22016.03.017.

Cinelli, S.D. and Kamel, A.H. 2013. Drilling Contractor. Low-cost radial jet drilling helps revitalize 40-year-old oilfield, http://www.drillingcontractor.org/low-cost-radial-jet-drilling-helps-revitalize-40-year-old-oilfield-23377(accessed 12 December 2015).

Dickinson, W. and Dickinson, R.W. 1985. Horizontal Radial Drilling System. Presented at the SPE California Regional Meeting, Bakersfield, California, 27—29 March. SPE-13949. http://dx.doi.org/10.2118/13949

Dickinson, W., Anderson, R.R., and Dickinson, R.W. 1986. The Ultrashort-Radius Radial System. Presented at the IADC/SPE Drilling Conference, Dallas, Texas, 10—12 February. SPE-14804. http://dx.doi.org/10.2118/14804.

Dickinson, W., Pesavento, M.J., and Dickinson, R.W. 1990. Data Acquisition, Analysis, And Control While Drilling With Horizontal Water Jet Drilling Systems. Presented at

the International Technical Meeting, Calgary, Canada, 10—13 June. SPE-90-127. http://dx.doi.org/10.2118/90-127.

Dickinson, W., Dykstra, H., Nordlund, R. et al. 1992. Coiled-Tubing Radials Placed by Water-Jet Drilling: Field Results, Theory, and Practice. Presented at the Annual Technical Conference and Exhibition, Houston, Texas, 3—6 October. SPE-26348. http://dx.doi.org/10.2118/26348.

Dickinson, W., Dykstra, H., and Nordlund, R. 1993. Coiled-Tubing Radials Placed by Water-Jet Drilling: Field Results, Theory, and Practice. Presented at the Annual Technical Conference and Exhibition, Houston, Texas, 3—6 October. SPE-26348. http://dx.doi.org/10.2118/26348.

Johansen, F.C. 1930. Flow through Pipe Orifices at Low Reynolds Numbers. Series A, Containing Papers of a Mathematical and Physical Character, *Proceedings of the Royal Society of London* 126 (801): 231—245. http:// www.jstor.org/stable/95350.

Kim, B.C., Cho, B.C., and Chi, N.H. 1997. Effects of Cavitation and Plate Thickness on Small Diameter Ratio Orifice Meters. *Flow Measurement and Instrumentation* 8 (2): 85—92. http://dx.doi.org/10.1016/S0955-5986(97)00034-4.

Kohar, J.P. and Gogoi, S. 2014. Radial Drilling Technique For Improving Recovery From Existing Oil Fields. *International Journal of Scientific & Technology Research* 3 (11): 159—161.

Li, J., Li, G., and Huang, Z. 2015. The self-propelled force model of a multi-orifice nozzle for radial jet drilling. *Journal of Natural Gas Science and Engineering* (24) 441—448.

Lichtarowicz, A., Duggins, R.K., and Markland, E. 1965. Discharge Coefficients for Incompressible, Non-Cavitating Flow through Long Orifices. *Journal of Mechanical Engineering Science* 7 (2): 210—219. http://dx.doi.org/10.1243/JMES_JOUR_1965_007_029_02.

Medaugh, F.W. and Johnson, G.D. 1940. Investigation of the Discharge and Coefficients of Small Circular Orifices. *Civil Engineering* 10 (7): 422—424.

Morris, G.K. and Garimella, S.V. 1998. Orifice and Impingement Flow Fields in Confined Jet Impingement. *ASME Journal of Electronic Packaging* 120 (1): 68—72. http://dx.doi.org/10.1115/1.2792288.

Nakayama, Y. 1961. Action of the fluid in the air micrometer: First report, characteristics of small diameter nozzle and orifice. *Bulletin Japan Society of Mechanical Engineers* 4 (1): 516—524. https://www.jstage.jst.go.jp/article/jsme1958/4/15/4_15_507/_pdf/-char/en.

Ragab, A.M. and Kamel, A.M. 2013. Radial Drilling Technique for Improving Well Productivity in Petrobel-Egypt. Presented at the North Africa Technical Conference&Exhibition, Cairo, Egypt, 15—17 April. SPE-164773. http://dx.doi.org/10.2118/164773.

Ramamurthi, K. and Nandakumar, K. 1999. Characteristics of Flow through Small Sharp-Edged Cylindrical Orifices. *Flow Measurement and Instrumentation* 10 (3): 133—143. http://dx.doi.org/10.1016/S0955-5986(99)00005-9.

Ruichang, G., Gensheng, L., and Zhongwei, H. 2009. Theoretical and experimental study of the pulling force of jet bits in radial drilling technology. *Petroleum Science* 6 (4): 395—399.

Ward-Smith, A.J. 1971. Pressure Losses in Ducted Flows. In A Unified Treatment of the Flow and Pressure Drop Characteristics of Constructions Having Orifices with Square Edges Chapt. 4. London, United Kingdom: Butterworths.

White, F.M. 1998. Integral Relations for a Control Volume. In Fluid Mechanics, fourth editionChapt. 3, 129—183. Boston, Massachusetts: McGraw-Hill series in Mechanical Engineering, WCB McGraw-Hill.

Yonghe, L., Chunjie, W., and Lianhai, S. 2000. Application and Development of Drilling and Completion of the Ultrashort-radius Radial Well by High Pressure Jet Flow Techniques. Presented at the SPE International Oil and Gas Conference and Exhibition, Bejing, China, 7—10 November. SPE-64756. http://dx.doi.org/10.2118/64756.

Appendix

Nozzle 1

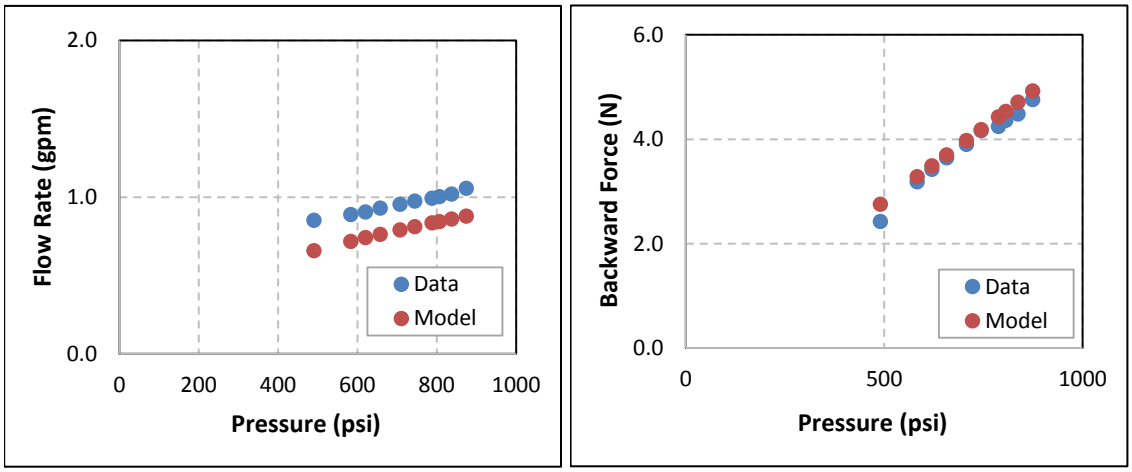

(a) **(b)**

Fig. A.1 – Results for Nozzle 1: a) flow rate vs. pressure; b) backward force vs. pressure
Number of orifices: 1
Orifice size: 0.893 mm
Aspect ratio: 2.575
Reynolds number: 180,000 - 250,000

Nozzle 2

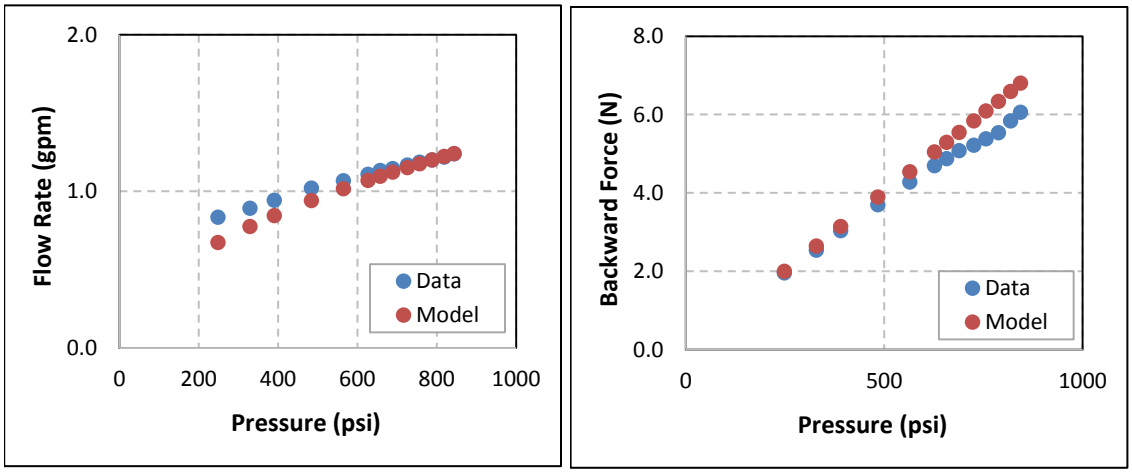

(a) **(b)**

Fig. A.2(a) – Results for Nozzle 2: a) flow rate vs. pressure plot; b) backward force vs. pressure
Number of orifices: 1
Orifice size: 1.073 mm
Aspect ratio: 2.097
Reynolds number: 130,000 - 250,000

Nozzle 3

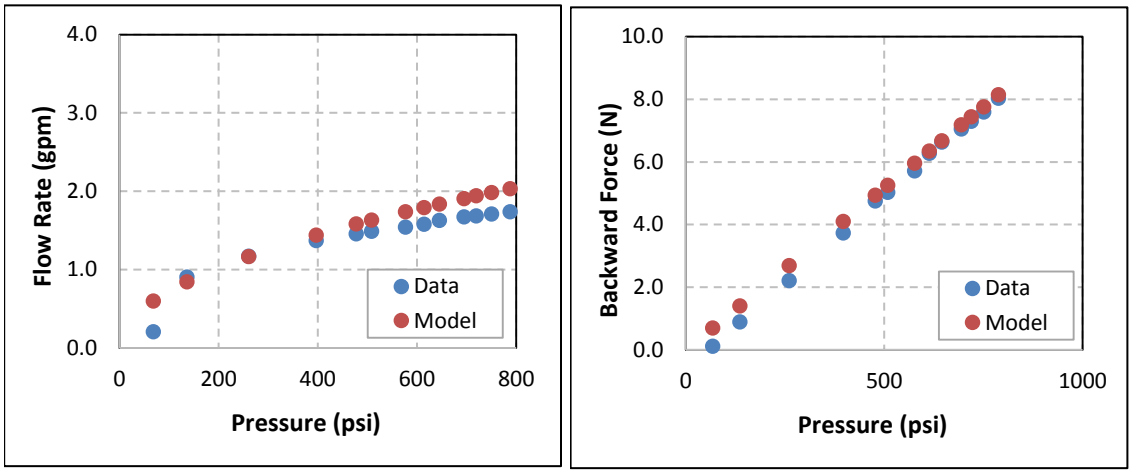

(a) **(b)**

Fig. A.3 – Results for Nozzle 3: a) flow rate vs. pressure plot; b) backward force vs. pressure

Number of orifices: 1
Orifice size: 1.406 mm
Aspect ratio: 1.64
Reynolds number: 70,000 - 240,000

Nozzle 5

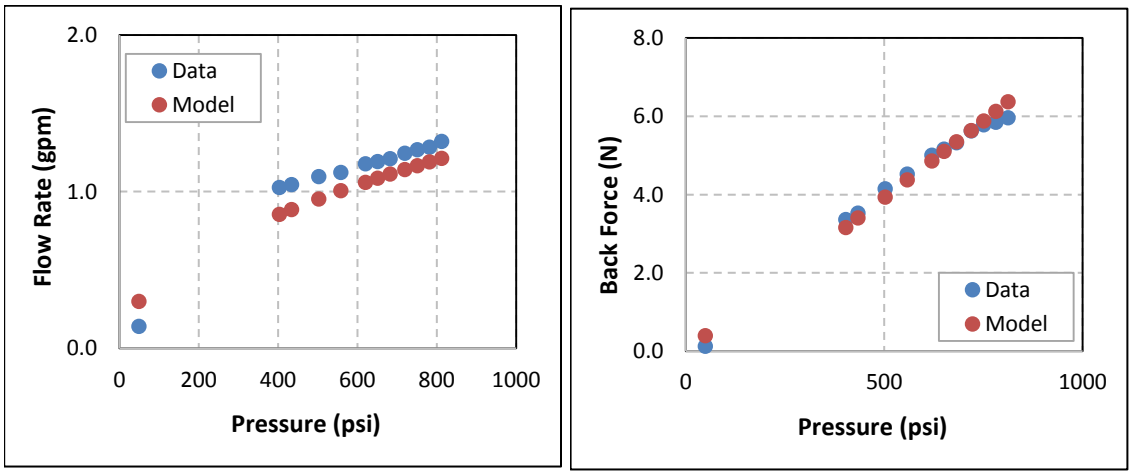

(a) **(b)**

Fig. A.4 – Results for Nozzle 5: a) flow rate vs. pressure; b) backward force vs. pressure

Number of orifices: 1
Orifice size: 1.084 mm
Aspect ratio: 6.31
Reynolds number: 175,000 - 705,000

Nozzle 7

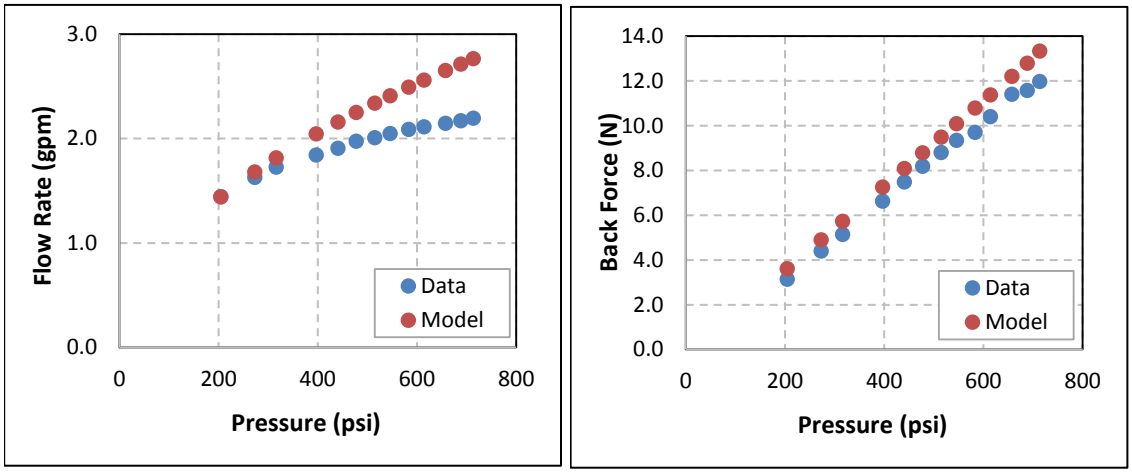

(a) **(b)**

Fig. A.5 – Results for Nozzle 7: a) flow rate vs. pressure; b) backward force vs. pressure
Number of orifices: 1
Orifice size: 1.706 mm
Aspect ratio: 4.48
Reynolds number: 400,000 - 760,000

Nozzle 8

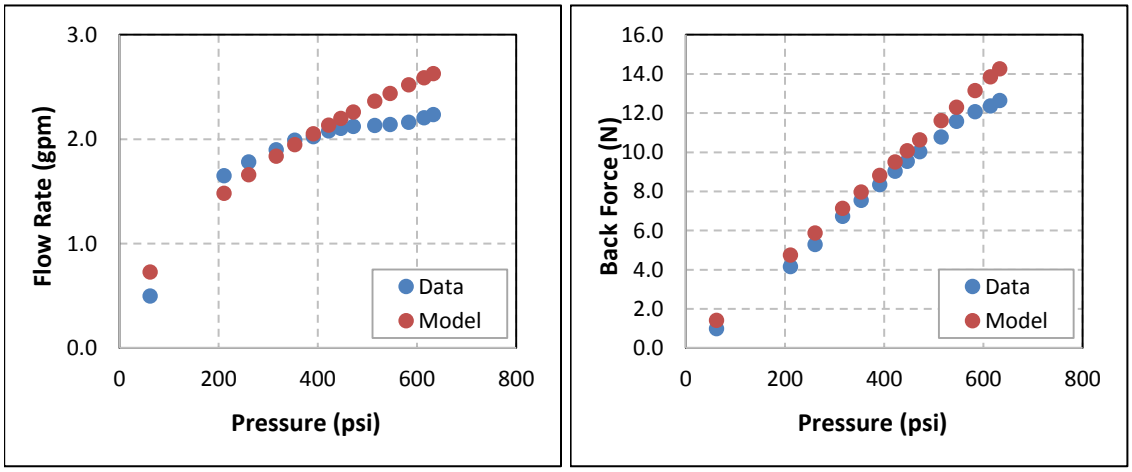

(a) **(b)**

Fig. A.6 – Results for Nozzle 8: a) flow rate vs. pressure; b) backward force vs. pressure
Number of orifices: 1
Orifice size: 1.838 mm
Aspect ratio: 3.92
Reynolds number: 200,000 - 760,000

Nozzle Combination 1

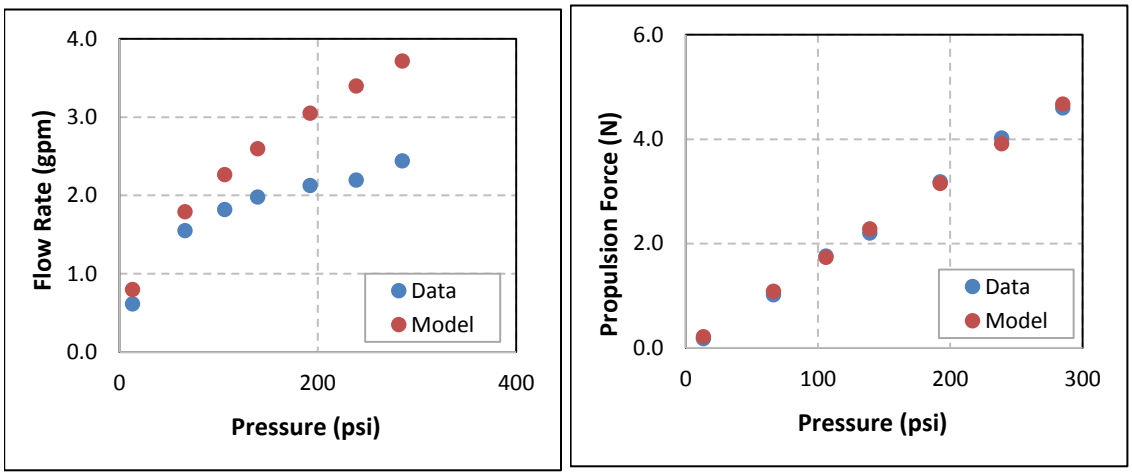

(a) **(b)**

Fig. A.7 – Results for Nozzle Combination 1: a) flow rate vs. pressure; b) propulsion force vs. pressure
Number of orifices: 3
Orifice size: 0.893mm (front), 1.6mm (back)
Flow rate: 0.6 - 3.8 gpm
Aspect ratio: 2.58 (front), 3.75 (back)

Nozzle Combination 2

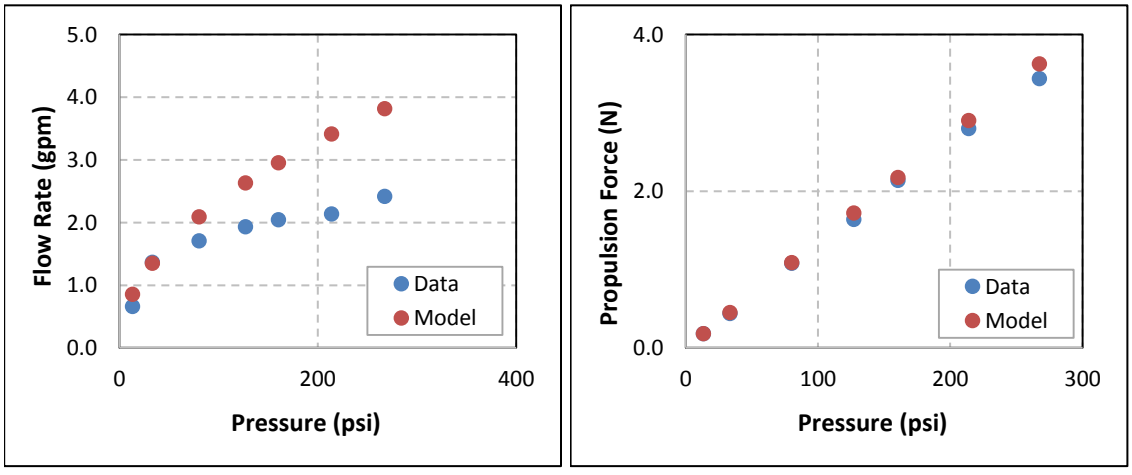

(a) **(b)**

Fig. A.8 – Results for Nozzle Combination 2: a) flow rate vs. pressure; b) propulsion force vs. pressure
Number of orifices: 3
Orifice size: 1.073mm (front), 1.6mm (back)
Aspect ratio: 2.10 (front), 3.75 (back)

Nozzle Combination 4

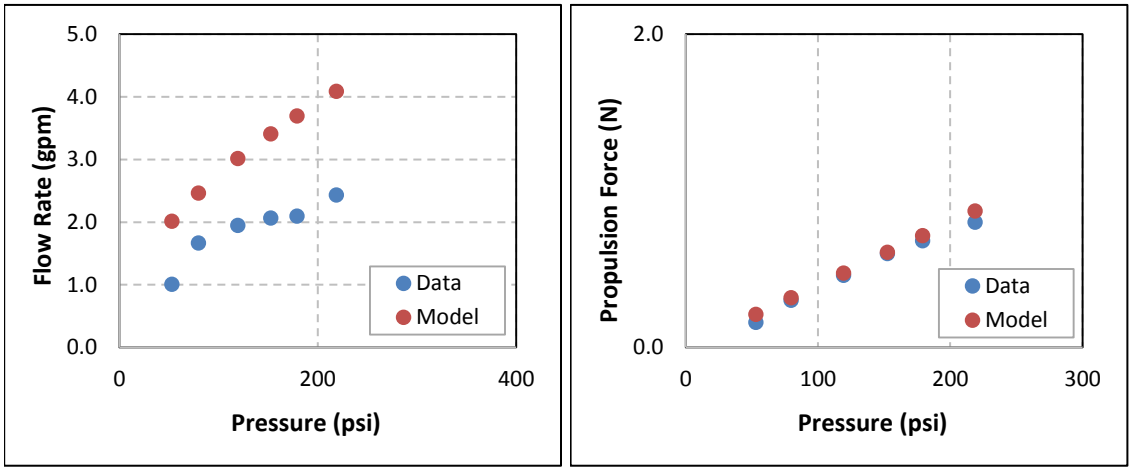

(a) **(b)**

Fig. A.9 – Results for Nozzle Combination 4: a) flow rate vs. pressure; b) propulsion force vs. pressure

Number of orifices: 3
Orifice size: 1.585mm (front), 1.6mm (back)
Aspect ratio: 1.45 (front), 3.75 (back)